

A HIGHER ORDER NONCONFORMING VIRTUAL ELEMENT METHOD FOR THE CAHN-HILLIARD EQUATION

ANDREAS DEDNER* AND ALICE HODSON*

Abstract. In this paper we develop a fully nonconforming virtual element method (VEM) of arbitrary approximation order for the two dimensional Cahn-Hilliard equation. We carry out the error analysis for the continuous-in-time scheme and verify the theoretical convergence result via numerical experiments. We present a fully discrete scheme which uses a convex splitting Runge-Kutta method to discretize in the temporal variable alongside the virtual element spatial discretization.

Key words. virtual element method, Cahn-Hilliard equation, nonlinear, fourth-order problems, nonconforming, DUNE.

AMS subject classifications. 65M12, 65M60

1. Introduction. Let $\Omega \subset \mathbb{R}^2$ denote a polygonal domain, with boundary $\partial\Omega$ and outward pointing normal n . Originally introduced by Cahn and Hilliard in [10, 11] to model the phase separation of a binary alloy, we consider the following two dimensional Cahn-Hilliard problem: find $u(x, t) : \Omega \times [0, T] \rightarrow \mathbb{R}$ such that

$$(1.1a) \quad \partial_t u - \Delta(\phi(u) - \varepsilon^2 \Delta u) = 0 \quad \text{in } \Omega \times (0, T],$$

$$(1.1b) \quad u(\cdot, 0) = u_0(\cdot) \quad \text{in } \Omega,$$

$$(1.1c) \quad \partial_n u = 0, \partial_n(\phi(u) - \varepsilon^2 \Delta u) = 0 \quad \text{on } \partial\Omega \times (0, T],$$

for time $T > 0$. We use the notation ∂_n for denoting the normal derivate and $\varepsilon > 0$ to represent the interface parameter. We define $\phi(x) = \psi'(x)$, where the free energy $\psi : \mathbb{R} \rightarrow \mathbb{R}$ is defined as

$$(1.2) \quad \psi(x) := \frac{1}{4}(1 - x^2)^2.$$

As described in [10, 11, 22], phase separation is a physical phenomenon occurring when a high temperature mixture is cooled down quickly and the two or more components in the mixture separate into regions of each one. As well as being used as a model for this type of phenomena, Cahn-Hilliard type equations have been used in a wide range of problems such as image processing [21], for example. Due to the numerous applications of the Cahn-Hilliard equation, there has been a lot of attention and research dedicated to numerical methods for problem (1.1).

Many classic methods used to solve the Cahn-Hilliard equation have been finite element (FE) based methods. These approaches can be split into two types, in the first, the equations are reformulated in mixed form, resulting in a system of second order problems which can be solved using classical methods suitable for elliptic problems, e.g., [25, 31]. The second approach involves solving the equations directly in their weak form, requiring the use of second order derivatives of the finite element functions. Solving the variational formulation of the fourth-order problem directly using FE methods is not straightforward due to the higher regularity requirements which have to be imposed on the finite element basis functions. Fully conforming methods [23, 26] require a large number of degrees of freedom even for the lowest

*Department of Mathematics, University of Warwick, Coventry, CV4 7AL, UK (a.s.dedner@warwick.ac.uk, alice-rachel.hodson@warwick.ac.uk).

order approximation or are based on sub triangulation. An easier approach is based on using suitable nonconforming spaces and to possibly include stabilization terms to achieve stability [14, 36]. A few nonconforming spaces have been suggested which have sufficient regularity to be stable without extra penalty terms [24, 37]. However, higher order versions of these spaces are not easily obtained. Consequently, there are few methods for fourth-order problems readily available in software packages, with most only providing the lowest order Morley element for these types of problems.

More recently, we have seen a handful of virtual element methods to discretize the Cahn-Hilliard equation [3, 33, 34]. The virtual element method is an extension and generalization of both finite element and mimetic difference methods. First introduced for second order elliptic problems in [8], virtual elements are highly desirable due to the straightforward way in which they extend to general polygonal meshes. The virtual element method is incredibly versatile and as such has been applied to a wide range of problems; for example, the development of higher order continuity spaces for the approximation of polyharmonic problems [5] as well as the construction of pointwise divergence-free spaces for the Stokes problem [7]. Other methods which have been considered for the discretization of problem (1.1) include the hybrid high-order (HHO) method (see [20] where the method was first introduced for a linear elasticity problem) as well as isogeometric analysis [29, 30]. In [13] an HHO approximation of the Cahn-Hilliard equation in mixed form is considered and, like the VEM approach, extends easily to general polygonal meshes.

A VEM discretization for problem (1.1) is considered in [3] where a C^1 conforming method is presented with only 3 degrees of freedom (dof) per vertex. Another conforming approach is considered in [33] however the problem is formulated in mixed form. Both works present a continuous-in-time (semidiscrete) convergence result for the lowest order VEM space. The only other application of the virtual element method to the Cahn-Hilliard equation is seen in [34] where a fully discrete scheme is presented and is shown to satisfy both a discrete energy law and a mass conservation law. In contrast to the virtual element discretizations developed in [3, 33, 34], we present the first analysis of a higher order VEM method and achieve optimal order error estimates for the semidiscrete scheme. A clear advantage of using higher order methods is the ability to use considerably lower grid resolutions which in turn can avoid the use of strongly adapted grids.

The aim of this paper is to present a new nonconforming virtual element method for the discretization of the Cahn-Hilliard equation. Our approach for constructing the VEM space follows [16]. We show that by defining the projection operators without using the underlying variational problem, we can directly apply our method to nonlinear fourth-order problems. Consequently, our approach does not require any special treatment of the nonlinearity as in [3]. Our method is shown to converge with optimal order also in the higher order setting. This projection approach has been implemented within the DUNE software framework [6, 18] requiring little change to the existing code base. To the best of our knowledge, this is the first analysis of a nonconforming virtual element method for the Cahn-Hilliard equation as well as the only higher order method without using a mixed formulation of (1.1).

This paper is organized in the following way. In section 2 we introduce the weak form of the continuous fourth-order Cahn-Hilliard problem, followed by the virtual element method discretization in section 3. In section 4 we carry out the error analysis of the continuous-in-time scheme before presenting numerical experiments to verify the theoretical results in section 5. Finally, we give proofs of some technical lemmas in Appendix A.

2. Problem formulation. We begin by introducing the variational formulation of problem (1.1) before introducing notation and some technicalities needed for the rest of the paper.

2.1. The continuous problem. First, we introduce the following space

$$V = H_0^2(\Omega) = \{v \in H^2(\Omega) : \partial_n v = 0 \text{ on } \partial\Omega\}.$$

Then, the variational form for (1.1) is described as follows: find $u(\cdot, t) \in V$ such that

$$(2.1) \quad \begin{aligned} (\partial_t u, v) + \varepsilon^2 a(u, v) + r(u; u, v) &= 0 \quad \forall v \in V \\ u(\cdot, 0) &= u_0(\cdot) \in V \end{aligned}$$

where the bilinear form $a(\cdot, \cdot)$ is the standard hessian form arising in the study of fourth-order problems

$$a(v, w) = (D^2 v, D^2 w) = \int_{\Omega} (D^2 v) : (D^2 w) \, dx = \int_{\Omega} \sum_{i,j=1}^2 \frac{\partial^2 v}{\partial x_i \partial x_j} \frac{\partial^2 w}{\partial x_i \partial x_j} \, dx$$

and the semilinear form $r(\cdot; \cdot, \cdot)$ is defined as

$$r(z; v, w) = \int_{\Omega} \phi'(z) Dv \cdot Dw \, dx$$

for all $z, v, w \in V$. Existence and uniqueness of a solution to problem (2.1) can be found in e.g. [24].

Note that we can view the Cahn-Hilliard equation as the H^{-1} gradient flow of the following free energy functional

$$(2.2) \quad E(u) = \int_{\Omega} \left(\psi(u) + \frac{\varepsilon^2}{2} |\nabla u|^2 \right) \, dx,$$

and notice that the total energy $E(u)$ decreases with time, $\frac{d}{dt} E(u(t)) \leq 0$.

2.2. Basic spaces and notation. Throughout this paper we use the notation $a \lesssim b$ to mean that $a \leq Cb$ for some constant C , which does not depend on h .

We denote the space of polynomials of degree less than or equal to ℓ on a set $K \subseteq \mathbb{R}^2$ by $\mathbb{P}_{\ell}(K)$. We denote a decomposition of the space Ω by \mathcal{T}_h and let h_K denote the diameter of a polygon $K \in \mathcal{T}_h$ where $\text{diam}(K) = \max_{x,y \in K} \|x - y\|$. We will denote the edges of a polygon $K \in \mathcal{T}_h$ by $e \subset \partial K$ and denote the set of all edges in \mathcal{T}_h by $\mathcal{E}_h = \mathcal{E}_h^{\text{int}} \cup \mathcal{E}_h^{\text{bdry}}$, split into boundary and internal edges respectively. Similarly, denote the set of vertices in \mathcal{T}_h by $\mathcal{V}_h = \mathcal{V}_h^{\text{int}} \cup \mathcal{V}_h^{\text{bdry}}$.

For an integer $s > 0$, define the *broken Sobolev space* $H^s(\mathcal{T}_h)$ by

$$H^s(\mathcal{T}_h) := \{v \in L^2(\Omega) : v|_K \in H^s(K), \forall K \in \mathcal{T}_h\},$$

and on this space define the inner product $(v_h, w_h)_{s,h} := \sum_{K \in \mathcal{T}_h} (D^s v_h, D^s w_h)_K$, with the broken H^s seminorm

$$|v_h|_{s,h}^2 := \sum_{K \in \mathcal{T}_h} |v_h|_{s,K}^2.$$

For a function $v \in H^2(\mathcal{T}_h)$ we define the jump operator $[\cdot]$ across an edge $e \in \mathcal{E}_h$ as follows. For an internal edge, $e \in \mathcal{E}_h^{\text{int}}$, define $[v] := v^+ - v^-$ where v^{\pm} denotes the trace of $v|_{K^{\pm}}$ where $e \subset \partial K^+ \cap \partial K^-$. For boundary edges, $e \in \mathcal{E}_h^{\text{bdry}}$, let $[v] := v|_e$.

DEFINITION 2.1. We define the H^2 -nonconforming space as follows.

$$H_\ell^{2,nc}(\mathcal{T}_h) := \left\{ v \in H^2(\mathcal{T}_h) : v \text{ continuous at internal vertices, } v(v^i) = 0 \ \forall v^i \in \mathcal{V}_h^{bdry}, \right. \\ \left. \int_e [\partial_n v] p \, ds = 0 \ \forall p \in \mathbb{P}_{\ell-2}(e), \int_e [v] p \, ds = 0 \ \forall p \in \mathbb{P}_{\ell-3}(e), \ \forall e \in \mathcal{E}_h \right\}.$$

As shown in e.g. [4, 16] it follows that the broken seminorm $|\cdot|_{2,h}$ is a norm on $H_\ell^{2,nc}(\mathcal{T}_h)$.

We also make the following regularity conditions on the mesh \mathcal{T}_h .

Assumption 2.2 (Mesh assumptions). Assume there exists some $\rho > 0$ such that the following hold. Let $K \in \mathcal{T}_h$.

- (A1) For every edge $e \subset \partial K$, $h_e \geq \rho h_K$ where $h_e = |e|$.
- (A2) Assume that K is star shaped with respect to a ball of radius ρh_K .
- (A3) There exists an interior point x_K to K such that the sub triangle formed by connecting x_K to the vertices of K is made of shape regular triangles.

Note that assumptions (A1) and (A2) are standard in the VEM framework (see e.g. [8]) however, assumption (A3), considered also in [4], is necessary for the proof of Lemma 4.8.

For any $K \in \mathcal{T}_h$ we define the orthogonal $L^2(K)$ projection onto the space $\mathbb{P}_\ell(K)$, that is $\mathcal{P}_\ell^K : L^2(K) \rightarrow \mathbb{P}_\ell(K)$, as the solution of

$$(\mathcal{P}_\ell^K v, p)_K = (v, p)_K \quad \forall p \in \mathbb{P}_\ell(K).$$

We also recall the following approximation results for the L^2 projection. A proof of the following can be obtained using for example the theory in [9].

THEOREM 2.3. Under (A1) and (A2) in Assumption 2.2, for $\ell \geq 0$ and for any $w \in H^m(K)$ with $1 \leq m \leq \ell + 1$, it follows that

$$|w - \mathcal{P}_\ell^K w|_{s,K} \lesssim h_K^{m-s} |w|_{m,K}$$

for $s = 0, 1, 2$. Further, for any edge shared by $K^+, K^- \in \mathcal{T}_h$ and for any $w \in H^m(K^+ \cup K^-)$, with $1 \leq m \leq \ell + 1$, it follows that

$$|w - \mathcal{P}_\ell^e w|_{s,e} \lesssim h_e^{m-s-\frac{1}{2}} |w|_{m,K^+ \cup K^-}$$

for $s = 0, 1, 2$.

Finally, we use the following notation for the local bilinear form $a^K(\cdot, \cdot)$. For $K \in \mathcal{T}_h$, define a^K as follows

$$a^K(v, w) = \int_K D^2 v : D^2 w \, dx \quad \forall v, w \in V.$$

3. Virtual element discretization. In this section we construct the VEM discretization. This involves building the discrete virtual element space, $V_{h,\ell}$, the projection operators, and the discrete forms. The first step in constructing the VEM space $V_{h,\ell}$ is to introduce an enlarged space $\tilde{V}_{h,\ell}^K$ and an extended set of dofs for this space. We then introduce a suitable set of dofs for $V_{h,\ell}^K$ and use these dofs to construct the *dof compatible* projection operators $\Pi_0^K, \Pi_1^K, \Pi_2^K$ which will be used to define the local VEM space as well as the local discrete forms. The projections have the advantage of being defined based on a constraint least squares problem and are fully computable using the dofs. Note that the construction is identical to the method employed in [16] where any omitted details can be found.

3.1. Local VEM space. Following the standard VEM enhancement technique [1, 12] we first give the definition of the local enlarged VEM space $\tilde{V}_{h,\ell}^K$ for $K \in \mathcal{T}_h$.

DEFINITION 3.1 (Local enlarged space). *Given an element $K \in \mathcal{T}_h$ define the local enlarged space $\tilde{V}_{h,\ell}^K$ as*

$$\tilde{V}_{h,\ell}^K = \{v_h \in H^2(K) : \Delta^2 v_h \in \mathbb{P}_\ell(K), v_h|_e \in \mathbb{P}_\ell(e), \Delta v_h|_e \in \mathbb{P}_{\ell-2}(e), \forall e \subset \partial K\}.$$

DEFINITION 3.2. *For $v_h \in H^2(K)$ and given integers d_0^e and d_0^i , we define the set of dofs $\Lambda^K(d_0^e, d_0^i)$ as the following.*

(D1) *The values of v_h at each vertex v of K .*

(D2) *The moments of v_h up to order d_0^e on each $e \subset \partial K$,*

$$\frac{1}{|e|} \int_e v_h p \, ds \quad \forall p \in \mathbb{P}_{d_0^e}(e).$$

(D3) *The moments of $\partial_n v_h$ up to order $\ell - 2$ on each $e \subset \partial K$,*

$$\int_e \partial_n v_h p \, ds \quad \forall p \in \mathbb{P}_{\ell-2}(e).$$

(D4) *The moments of v_h up to order d_0^i inside K ,*

$$\frac{1}{|K|} \int_K v_h p \, dx \quad \forall p \in \mathbb{P}_{d_0^i}(K).$$

Remark 3.3. Adopting the notation in [16], we point out that a set of dofs $\Lambda^K(d_0^e, d_0^i)$ described by Definition 3.2 corresponds to the dof tuple $(0, -1, d_0^e, \ell - 2, d_0^i)$.

For a set of dofs described by Definition 3.2, we fix (D1) as function values at the vertices of K and we fix edge normal moments up to $\ell - 2$ in (D3). We then define the edge moments up to order d_0^e in (D2) and define inner moments up to order d_0^i in (D4). The local enlarged space (Definition 3.1) is therefore characterized by the extended set of degrees of freedom $\Lambda^K(\ell - 2, \ell)$. This set of dofs is unisolvent over the space $\tilde{V}_{h,\ell}^K$ [16]. The local VEM space $V_{h,\ell}^K \subset \tilde{V}_{h,\ell}^K$ is characterized by taking $d_0^e = \ell - 3$ and $d_0^i = \ell - 4$ in Definition 3.2, to get a set of dofs $\Lambda^K(\ell - 3, \ell - 4)$. Note that this set of dofs is identical to the set used in [4] for the biharmonic problem and they are visualized on triangles in Figure 1.

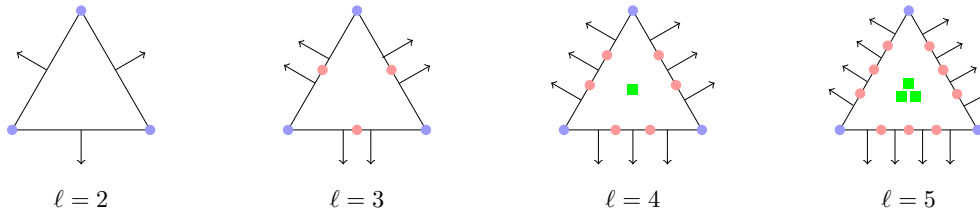


FIG. 1. Degrees of freedom for polynomial orders $\ell = 2, 3, 4, 5$ on triangles for the local VEM space. Circles at vertices represent vertex dofs, arrows represent edge normal dofs, circles on edges represent edge value moments and interior squares represent inner dofs.

In order to define the local VEM space we now introduce the following projection operators: an interior value projection $\Pi_0^K : \tilde{V}_{h,\ell}^K \rightarrow \mathbb{P}_\ell(K)$, an edge value projection $\Pi_0^e : \tilde{V}_{h,\ell}^K \rightarrow \mathbb{P}_\ell(e)$, and finally an edge normal projection $\Pi_1^e : \tilde{V}_{h,\ell}^K \rightarrow \mathbb{P}_{\ell-1}(e)$. As in [16] we consider projection operators obtained from the following constraint least squares problem.

DEFINITION 3.4 (Projection operators). *We define the symmetric, positive definite stabilization bilinear form $S_K(\cdot, \cdot)$ as follows*

$$(3.1) \quad S_K(v_h, w_h) := \sum_{\lambda_j \in \Lambda^K(\ell-3, \ell-4)} \lambda_j(v_h) \lambda_j(w_h) \quad \forall v_h, w_h \in \tilde{V}_{h,\ell}^K.$$

We define the value projection $\Pi_0^K v_h$ as the solution to the problem

$$\begin{aligned} \text{Minimize:} \quad & S_K(\Pi_0^K v_h - v_h, \Pi_0^K v_h - v_h), \\ \text{subject to:} \quad & \int_K \Pi_0^K v_h p \, dx = \int_K v_h p \, dx \quad \forall p \in \mathbb{P}_{\ell-4}(K). \end{aligned}$$

We define the edge projection as the unique solution in $\mathbb{P}_\ell(e)$ of

$$\begin{aligned} \int_e \Pi_0^e v_h p \, ds &= \int_e v_h p \, ds \quad \forall p \in \mathbb{P}_{\ell-3}(e), \\ \int_e \Pi_0^e v_h p \, ds &= \int_e \Pi_0^K v_h p \, ds \quad \forall p \in \mathbb{P}_{\ell-2}(e) \setminus \mathbb{P}_{\ell-3}(e), \\ \Pi_0^e v_h(e^\pm) &= v_h(e^\pm). \end{aligned}$$

We define the normal edge projection as the unique solution in $\mathbb{P}_{\ell-1}(e)$ of

$$\int_e \Pi_1^e v_h p \, ds = \int_e \partial_n v_h p \, ds \quad \forall p \in \mathbb{P}_{\ell-2}(e).$$

Finally, we are able to use the projections defined in Definition 3.4 to define both the gradient Π_1^K and hessian Π_2^K projections.

DEFINITION 3.5. *The gradient projection $\Pi_1^K : \tilde{V}_{h,\ell}^K \rightarrow (\mathbb{P}_{\ell-1}(K))^2$ is defined as*

$$\int_K \Pi_1^K v_h p \, dx = - \int_K \Pi_0^K v_h \nabla p \, dx + \sum_{e \subset \partial K} \int_e \Pi_0^e v_h p n \, ds,$$

for all $p \in (\mathbb{P}_{\ell-1}(K))^2$. The hessian projection $\Pi_2^K : \tilde{V}_{h,\ell}^K \rightarrow (\mathbb{P}_{\ell-2}(K))^{2 \times 2}$ is defined as

$$\int_K \Pi_2^K v_h p \, dx = - \int_K \Pi_1^K v_h \otimes \nabla p \, dx + \sum_{e \subset \partial K} \int_e (\Pi_1^e v_h n \otimes np + \partial_s(\Pi_0^e v_h) \tau \otimes np) \, ds,$$

for all $p \in (\mathbb{P}_{\ell-2}(K))^{2 \times 2}$. Here n, τ denote the unit normal and tangent vectors of e , respectively.

By defining the projections in this way, it follows that they are indeed computable from the dofs [16]. Using Definition 3.4 we can now define the local virtual space. This is given as follows.

DEFINITION 3.6 (Local virtual space). *The local virtual element space $V_{h,\ell}^K$ is defined as*

$$(3.2) \quad V_{h,\ell}^K := \left\{ v_h \in \tilde{V}_{h,\ell}^K : (v_h - \Pi_0^K v_h, p)_K = 0 \quad \forall p \in \mathbb{P}_\ell(K) \setminus \mathbb{P}_{\ell-4}(K), \right. \\ \left. (v_h - \Pi_0^e v_h, p)_e = 0 \quad \forall p \in \mathbb{P}_{\ell-2}(e) \setminus \mathbb{P}_{\ell-3}(e) \right\}.$$

The set of local degrees of freedom $\Lambda^K(\ell - 3, \ell - 4)$ is unisolvent over $V_{h,\ell}^K$. A proof of this can be found in [16]. Also shown in [16] is the proof of the subsequent lemma, detailing that all the projections satisfy a crucial L^2 projection property. This property follows as a consequence of the construction of the value, gradient, and hessian projections.

LEMMA 3.7. *The value, gradient, and hessian projections satisfy*

$$(3.3) \quad \Pi_s^K v_h = \mathcal{P}_{\ell-s}^K(D^s v_h) \quad \forall v_h \in V_{h,\ell}^K,$$

for $s = 0, 1, 2$. It also holds that $\mathbb{P}_\ell(K) \subset V_{h,\ell}^K$ and therefore

$$(3.4) \quad \Pi_s^K p = D^s p \quad \forall p \in \mathbb{P}_\ell(K),$$

for $s = 0, 1, 2$.

3.2. Global spaces and the discrete forms. The global VEM space can now be defined in the standard way as follows.

DEFINITION 3.8 (Global virtual space). *The global VEM space is defined as*

$$(3.5) \quad V_{h,\ell} := \left\{ v_h \in H_\ell^{2,nc}(\mathcal{T}_h) : v_h|_K \in V_{h,\ell}^K \quad \forall K \in \mathcal{T}_h \right\}$$

where $H_\ell^{2,nc}(\mathcal{T}_h)$ is the nonconforming space given in Definition 2.1.

As usual, we can define the corresponding global dofs as an extension to those described in Definition 3.2 with $d_0^e = \ell - 3$ and $d_0^i = \ell - 4$. We can extend (D1) to evaluation at internal vertices, (D2) and (D3) to internal edges $e \in \mathcal{E}_h^{\text{int}}$, and finally we can take (D4) for each $K \in \mathcal{T}_h$. We set the local dofs which correspond to boundary vertices and boundary edges to zero. Note that the global degrees of freedom are unisolvent - this follows from the unisolvency of the local degrees of freedom and the definition of the local spaces.

Now that we have the virtual spaces and the projection operators, we are able to define the discrete bilinear forms, the last step in the VEM construction.

DEFINITION 3.9 (Discrete forms). *For $v_h, w_h, z_h \in V_{h,\ell}$ define the discrete forms as*

$$a_h^K(v_h, w_h) = \int_K \Pi_2^K v_h : \Pi_2^K w_h \, dx + h_K^{-2} S_K(v_h - \Pi_0^K v_h, w_h - \Pi_0^K w_h), \\ m_h^K(v_h, w_h) = \int_K \Pi_0^K v_h \Pi_0^K w_h \, dx + h_K^2 S_K(v_h - \Pi_0^K v_h, w_h - \Pi_0^K w_h), \\ r_h^K(z_h; v_h, w_h) = \int_K \phi'(z_h) \Pi_1^K v_h \cdot \Pi_1^K w_h \, dx + \beta_K S_K(v_h - \Pi_0^K v_h, w_h - \Pi_0^K w_h),$$

where $S_K(\cdot, \cdot)$ has been defined previously in (3.1), and β_K is constant. Due to Lemma 3.7, it is immediate that the discrete forms possess the standard consistency property, which tells us that whenever one of the entries in the bilinear form is a polynomial of degree ℓ , the form is exact.

LEMMA 3.10 (Polynomial consistency). *For any $w_h \in V_{h,\ell}$, it holds that*

$$a_h^K(p, w_h) = a^K(p, w_h), \quad m_h^K(p, w_h) = (p, w_h)_K$$

for all $p \in \mathbb{P}_\ell(K)$.

We also have the standard stability property for the forms, the proof can be found for example in [12].

LEMMA 3.11 (Stability). *There exists positive constants α_* , α^* , μ_* , and μ^* such that for all $v_h \in V_{h,\ell}^K$*

$$\begin{aligned} \alpha_* a^K(v_h, v_h) &\leq a_h^K(v_h, v_h) \leq \alpha^* a^K(v_h, v_h) \\ \mu_* (v_h, v_h)_K &\leq m_h^K(v_h, v_h) \leq \mu^* (v_h, v_h)_K. \end{aligned}$$

The global forms can be defined in the usual way, for $z_h, v_h, w_h \in V_{h,\ell}$,

$$\begin{aligned} a_h(v_h, w_h) &:= \sum_{K \in \mathcal{T}_h} a_h^K(v_h, w_h), \quad m_h(v_h, w_h) := \sum_{K \in \mathcal{T}_h} m_h^K(v_h, w_h), \\ r_h(z_h; v_h, w_h) &:= \sum_{K \in \mathcal{T}_h} r_h^K(z_h; v_h, w_h). \end{aligned}$$

Finally, we assume that there exists the interpolation operator I_h , defined in the usual way, which satisfies interpolation estimates, i.e. for any $w \in H^m(K)$ with $1 \leq m \leq \ell + 1$ it holds that

$$(3.6) \quad |w - I_h w|_{s,K} \lesssim h^{m-s} |w|_{m,K}$$

for $s = 0, 1, 2$.

4. Error analysis of the semidiscrete scheme. This section details the error analysis for the continuous-in-time (semidiscrete) scheme, presented in (4.1). We begin by introducing the scheme before proving L^2 convergence in Theorem 4.9. Note that we only deal with the analysis in the semidiscrete case since standard arguments can be employed in the fully discrete case, and the aim and focus of this paper is the VEM spatial discretization. Throughout this section we assume that $\ell \geq 2$.

4.1. The semidiscrete problem. The semidiscrete problem is defined as follows: find $u_h(\cdot, t) \in V_{h,\ell}$ such that

$$(4.1) \quad \begin{aligned} m_h(\partial_t u_h, v_h) + \varepsilon^2 a_h(u_h, v_h) + r_h(\Pi_0^K(u_h); u_h, v_h) &= 0 \quad \forall v_h \in V_{h,\ell}, \text{ a.e. } t \text{ in } (0, T), \\ u_h(\cdot, 0) &= u_{h,0}(\cdot) \in V_{h,\ell} \end{aligned}$$

where $u_{h,0}$ is some approximation of u_0 and the discrete forms are given in Definition 3.9.

We make the following assumption on the discrete solution u_h of (4.1), for more details on this assumption and for a full justification see [24].

Assumption 4.1. The solution u_h to (4.1) satisfies for all $t \in (0, T]$

$$\|u_h(\cdot, t)\|_{1,\infty;h} \leq C_T$$

for a constant C_T independent of h , which depends on T , where

$$\|v_h\|_{m,\infty;h} := \max_{\substack{1 \leq j \leq m \\ K \in \mathcal{T}_h}} |v_h|_{j,\infty,K}.$$

4.2. The elliptic projection. In this subsection we introduce the elliptic projection, which is fundamental for the proof of Theorem 4.9. We define the elliptic projection $P_h v \in V_{h,\ell}$ for $v \in H^4(\Omega)$ as the solution of

$$(4.2) \quad b_h(P_h v, \psi_h) = (\varepsilon^2 \Delta^2 v - \nabla \cdot (\phi'(u) \nabla v) + \alpha v, \psi_h) \quad \forall \psi_h \in V_{h,\ell}$$

where the bilinear form $b_h(\cdot, \cdot)$ is defined as

$$(4.3) \quad b_h(v_h, w_h) := \varepsilon^2 a_h(v_h, w_h) + r_h(u; v_h, w_h) + \alpha(v_h, w_h),$$

for a positive α , chosen so that the bilinear form b_h is coercive. Before we state some approximation properties of P_h , we require the following lemma, the proof of which can be found in [16].

LEMMA 4.2. *For the solution u to (2.1) and for $w \in H_\ell^{2,nc}(\mathcal{T}_h)$, we define the nonconformity error as follows*

$$(4.4) \quad \mathcal{N}(u, w) = \varepsilon^2 (a(u, w) - (\Delta^2 u, w)),$$

and it satisfies the following

$$(4.5) \quad |\mathcal{N}(u, w)| = \left| \varepsilon^2 \sum_{K \in \mathcal{T}_h} \int_{\partial K} ((\Delta u - \partial_{ss} u) \partial_n w + \partial_{ns} u \partial_s w - \partial_n (\Delta u) w) \, ds \right| \lesssim h^{\ell-1} |w|_{2,h}.$$

LEMMA 4.3. *Let u be the solution to (2.1) and let $P_h u$ be the elliptic projection defined in (4.2). Then, it holds that*

$$(4.6) \quad \|u - P_h u\|_{2,h} \lesssim h^{\ell-1},$$

$$(4.7) \quad \|u - P_h u\|_{1,h} \lesssim h^\ell,$$

$$(4.8) \quad \|u_t - (P_h u)_t\|_{2,h} \lesssim h^{\ell-1},$$

$$(4.9) \quad \|u_t - (P_h u)_t\|_{1,h} \lesssim h^\ell.$$

Proof of the estimate (4.6) in Lemma 4.3 is a direct consequence of the energy norm convergence proof covered in [16, Theorem 5.7] for a general fourth-order problem with varying coefficients.

In order to prove (4.7) we first study the following problem: find $z \in V$ such that

$$(4.10) \quad b(z, w) = (u - P_h u, w)_{1,h} + (u - P_h u, w)_{0,h} =: L_h(w) \quad \forall w \in V$$

where the bilinear form $b(\cdot, \cdot)$ is defined as

$$b(v, w) := \varepsilon^2 a(v, w) + r(u; v, w) + \alpha(v, w)$$

for all $v, w \in V$. Then it follows from [24] that there exists a solution and the following regularity result holds for $z \in H^3(\Omega)$

$$(4.11) \quad \|z\|_{3,\Omega} \lesssim \|u - P_h u\|_{1,h}.$$

LEMMA 4.4. *Let u be the solution to (2.1) and let $P_h u$ be the elliptic projection defined in (4.2). For the solution $z \in H^3(\Omega)$ of the dual problem (4.10), it holds that*

$$(4.12) \quad |b(z, u - P_h u)| \lesssim h^\ell \|u - P_h u\|_{1,h}.$$

We give the proof of Lemma 4.4 in Appendix A. Also necessary for the proof of (4.8)-(4.9) in Lemma 4.3 is the following lemma, the proof is given in Appendix A.

LEMMA 4.5. *Let u be the solution to (2.1) and let $P_h u$ be the elliptic projection defined in (4.2). For any $\eta_h \in V_{h,\ell}$, it holds*

$$|(\phi''(u)u_t \Pi_1^K P_h u, \Pi_1^K \eta_h)_{0,h} - (\phi''(u)u_t \nabla u, \nabla \eta_h)_{0,h}| \lesssim h^\ell \|\eta_h\|_{2,h}.$$

We now give the proof of Lemma 4.3.

Proof of Lemma 4.3. Define $\rho := u - P_h u$. Then, it follows that

$$\|\rho\|_{1,h}^2 = (l_h(\rho) - b(z, \rho)) + b(z, \rho) = I + II.$$

In view of Lemma 4.4 we need only estimate term I .

To this end, we introduce the interpolation $I_h^1 \rho =: \rho_I$ of ρ into the lowest order C^1 -conforming VEM space, i.e. $\rho_I \in V$. Then, $b(z, \rho_I) - l_h(\rho_I) = 0$. Therefore

$$I = l_h(\rho) - b(z, \rho) + b(z, \rho_I) - l_h(\rho_I) \leq |l_h(\rho - \rho_I)| + |b(z, \rho_I - \rho)|.$$

Firstly, using Cauchy-Schwarz, properties of the lowest order conforming interpolation, and (4.6), it holds that

$$\begin{aligned} |l_h(\rho - \rho_I)| &= \left| \sum_{K \in \mathcal{T}_h} \int_K \nabla \rho \cdot \nabla (\rho - \rho_I) + \rho(\rho - \rho_I) \, dx \right| \\ &\lesssim h \|u - P_h u\|_{1,h} \|u - P_h u\|_{2,h} \lesssim h^\ell \|u - P_h u\|_{1,h}. \end{aligned}$$

Secondly, using the definition of $b(\cdot, \cdot)$

$$b(z, \rho_I - \rho) = \varepsilon^2 (D^2 z, D^2 (\rho_I - \rho)) + r(u; z, \rho_I - \rho) + \alpha(z, \rho_I - \rho).$$

We also note that after an application of integration by parts, we have that

$$\begin{aligned} |\varepsilon^2 (D^2 z, D^2 (\rho_I - \rho))| &\leq |\varepsilon^2 (\nabla \Delta z, \nabla (\rho_I - \rho))| \\ &\quad + \varepsilon^2 \left| \sum_{K \in \mathcal{T}_h} \int_{\partial K} ((\Delta z - \partial_{ss} z) \partial_n \rho + \partial_{ns} z \partial_s \rho) \, ds \right|. \end{aligned}$$

Notice that the second term above can be estimated using the same method as in Lemma 4.2, the proof of which can be found in [16, Theorem 5.5], and therefore

$$(4.13) \quad |\varepsilon^2 (D^2 z, D^2 (\rho_I - \rho))| \lesssim \varepsilon^2 \|z\|_{3,\Omega} h \|u - P_h u\|_{2,h} \lesssim h^\ell \|u - P_h u\|_{1,h},$$

where we have used (4.6), and (4.11). Similarly, we can show that

$$(4.14) \quad |r(u; z, \rho_I - \rho)| \lesssim h \|z\|_{3,\Omega} \|u - P_h u\|_{2,h} \lesssim h^\ell \|u - P_h u\|_{1,h}$$

$$(4.15) \quad |\alpha(z, \rho_I - \rho)| \lesssim h \|z\|_{3,\Omega} \|u - P_h u\|_{2,h} \lesssim h^\ell \|u - P_h u\|_{1,h}.$$

Therefore combining (4.13), (4.14), and (4.15),

$$I \lesssim h^\ell \|u - P_h u\|_{1,h}.$$

Therefore (4.7) holds.

It remains to show (4.8)-(4.9). For this, we notice that for any $w_h \in V_{h,\ell}$

$$(4.16) \quad \begin{aligned} b_h((P_h u)_t, w_h) &= b(u_t, w_h) - \mathcal{N}(u_t, w_h) \\ &\quad + (\phi''(u)u_t \nabla u, \nabla w_h) - (\phi''(u)u_t \Pi_1^K P_h u, \Pi_1^K w_h). \end{aligned}$$

Using the coercivity of the bilinear form b_h , alongside (4.16) and the definition of $P_h u$, we have the following

$$\begin{aligned} \|P_h(u_t) - (P_h u)_t\|_{2,h}^2 &\lesssim b_h(P_h(u_t) - (P_h u)_t, P_h(u_t) - (P_h u)_t) \\ &= b_h(P_h(u_t), P_h(u_t) - (P_h u)_t) - b_h((P_h u)_t, P_h(u_t) - (P_h u)_t) \\ &= (\phi''(u)u_t \Pi_1^K P_h u, \Pi_1^K (P_h(u_t) - (P_h u)_t)) - (\phi''(u)u_t \nabla u, \nabla (P_h(u_t) - (P_h u)_t)) \\ &\lesssim h^\ell \|P_h(u_t) - (P_h u)_t\|_{2,h} \end{aligned}$$

where we have applied Lemma 4.5 with $\eta_h = P_h(u_t) - (P_h u)_t$ in the last step. It therefore follows that

$$\|u_t - (P_h u)_t\|_{2,h} \leq \|u_t - P_h(u_t)\|_{2,h} + \|P_h(u_t) - (P_h u)_t\|_{2,h} \lesssim h^{\ell-1}.$$

In order to prove (4.9), we proceed in the exact same way as the proof of (4.7). We consider again a dual problem: find $\tilde{z} \in V$ such that

$$b(\tilde{z}, w) = (u_t - (P_h u)_t, w)_{1,h} + (u_t - (P_h u)_t, w)_{0,h} \quad \forall w \in V.$$

We can then use Lemma 4.5 with $\eta_h = I_h \tilde{z}$ as well as a regularity result for \tilde{z} to show that

$$|b(\tilde{z}, u_t - (P_h u)_t)| \lesssim h^\ell \|u_t - (P_h u)_t\|_{1,h}$$

and the result follows as before. \square

Remark 4.6. Notice that it follows from (3.6), (4.7) as well as stability properties of the interpolation operator that the elliptic projection is bounded [24]. In particular,

$$(4.17) \quad \|P_h u\|_{1,\infty,h} \leq C.$$

We require one more result before we can prove the L^2 error estimate in Theorem 4.9, an estimate for the semilinear term r_h . We use the following standard error decomposition arising in the study of time-dependent problems

$$(4.18) \quad u - u_h = (u - P_h u) + (P_h u - u_h) =: \rho + \theta,$$

for the solution u to (2.1) and for the projection $P_h u$ defined in (4.2).

LEMMA 4.7. *Suppose that $u \in H^{\ell+1}(\Omega)$ solves (2.1) and that $P_h u$ is the projection defined in (4.2). Then, it follows that*

$$(4.19) \quad |r_h(\Pi_0^K u_h; u_h, \theta) - r_h(u; P_h u, \theta)| \lesssim (\|\theta\|_{0,h} + \|\rho\|_{0,h} + h^\ell) |\theta|_{1,h}.$$

Proof. Using the definition of r_h we have that

$$\begin{aligned} &|r_h(\Pi_0^K u_h; u_h, \theta) - r_h(u; P_h u, \theta)| \\ &= \left| \sum_{K \in \mathcal{T}_h} \int_K (\phi'(\Pi_0^K u_h) \Pi_1^K u_h - \phi'(u) \Pi_1^K (P_h u)) \cdot \Pi_1^K \theta \, dx \right| \end{aligned}$$

$$\leq \sum_{K \in \mathcal{T}_h} \|\phi'(\Pi_0^K u_h) \Pi_1^K u_h - \phi'(u) \Pi_1^K(P_h u)\|_{0,K} |\theta|_{1,K}$$

where we have used Lemma 3.7 since $\theta \in V_{h,\ell}$. Therefore, using the triangle inequality, we see that

$$\begin{aligned} \|\phi'(\Pi_0^K u_h) \Pi_1^K u_h - \phi'(u) \Pi_1^K(P_h u)\|_{0,K} &\leq \|\phi'(\Pi_0^K u_h) (\Pi_1^K u_h - \Pi_1^K(P_h u))\|_{0,K} \\ &\quad + \|(\phi'(\Pi_0^K u_h) - \phi'(u)) \Pi_1^K(P_h u)\|_{0,K} \\ &= J_1 + J_2. \end{aligned}$$

To estimate the first term it follows that

$$J_1 = \|\phi'(\Pi_0^K u_h) (\Pi_1^K u_h - \Pi_1^K(P_h u))\|_{0,K} = \|\phi'(\Pi_0^K u_h) \Pi_1^K \theta\|_{0,\Omega} \lesssim |\theta|_{1,K}$$

where we have used Assumption 4.1, alongside L^∞ stability properties of the L^2 projection (for more details see e.g. the theory in [15]).

To estimate the second term, it follows that

$$J_2 = \|(\phi'(\Pi_0^K u_h) - \phi'(u)) \Pi_1^K(P_h u)\|_{0,K} \lesssim \|P_h u\|_{1,\infty;h} \|\Pi_0^K u_h - u\|_{0,K}$$

where we have used the bounded property of $P_h u$ in (4.17).

Notice that using the triangle inequality, the definitions of ρ, θ , and properties of the L^2 projection, we observe

$$\begin{aligned} \|\Pi_0^K u_h - u\|_{0,K} &\leq \|\Pi_0^K u_h - \Pi_0^K P_h u\|_{0,K} + \|\mathcal{P}_\ell^K P_h u - \mathcal{P}_\ell^K u\|_{0,K} + \|\mathcal{P}_\ell^K u - u\|_{0,K} \\ &= \|\Pi_0^K \theta\|_{0,K} + \|\mathcal{P}_\ell^K \rho\|_{0,K} + \|(I - \mathcal{P}_\ell^K)u\|_{0,K} \\ &\lesssim (\|\theta\|_{0,K} + \|\rho\|_{0,K} + h^\ell |u|_{\ell,K}). \end{aligned}$$

Hence by combining the estimates for J_1 and J_2 we have that

$$|r_h(\Pi_0^K u_h; u_h, \theta) - r_h(u, P_h u, \theta)| \lesssim (|\theta|_{1,h} + \|\theta\|_{0,h} + \|\rho\|_{0,h} + h^\ell) |\theta|_{1,h}$$

as required. \square

4.3. Error estimate for the semidiscrete scheme. In this subsection we prove the error estimate for the scheme detailed in (4.1). Note that in the following we do not include the dependence of u and u_h on time t .

In order to present the convergence result we require one additional lemma. The proof is given in Appendix A.

LEMMA 4.8. *For any $w_h, z_h \in V_{h,\ell}$, it holds that*

$$(4.20) \quad \left| \sum_{K \in \mathcal{T}_h} \int_{\partial K} (\partial_n z_h) w_h \, ds \right| \lesssim h (|w_h|_{1,h} |z_h|_{2,h} + |w_h|_{2,h} |z_h|_{2,h}).$$

We now present the main L^2 convergence theorem.

THEOREM 4.9. *Assume that u is the solution to the continuous problem (2.1) and u_h is the solution to (4.1). Then, for all $t \in [0, T]$,*

$$(4.21) \quad \|u - u_h\|_{0,h} \lesssim h^\ell.$$

Proof. Recall the error decomposition detailed in (4.18), and notice that due to Lemma 4.3, we need only estimate θ . Following the ideas in [3], we use the definition of θ and the semidiscrete scheme (4.1) to show that

$$\begin{aligned} m_h(\theta_t, \chi_h) + \varepsilon^2 a_h(\theta, \chi_h) &= m_h((P_h u)_t, \chi_h) + \varepsilon^2 a_h(P_h u, \chi_h) \\ &\quad - (m_h((u_h)_t, \chi_h) + \varepsilon^2 a_h(u_h, \chi_h)) \\ (4.22) \qquad \qquad \qquad &= m_h((P_h u)_t, \chi_h) + \varepsilon^2 a_h(P_h u, \chi_h) + r_h(\Pi_0^K u_h; u_h, \chi_h). \end{aligned}$$

Using the definition of the elliptic projection in (4.2) and (4.3), it follows that

$$\begin{aligned} \varepsilon^2 a_h(P_h u, \chi_h) &= b_h(P_h u, \chi_h) - r_h(u; P_h u, \chi_h) - \alpha(P_h u, \chi_h) \\ &= (\varepsilon^2 \Delta^2 u - \nabla \cdot (\phi'(u) \nabla u) + \alpha u, \chi_h) - r_h(u; P_h u, \chi_h) - \alpha(P_h u, \chi_h). \end{aligned}$$

Therefore, substituting this into (4.22) we see that

$$\begin{aligned} (4.23) \qquad m_h(\theta_t, \chi_h) + \varepsilon^2 a_h(\theta, \chi_h) &= m_h((P_h u)_t, \chi_h) + (\varepsilon^2 \Delta^2 u - \nabla \cdot (\phi'(u) \nabla u), \chi_h) \\ &\quad + \alpha(u - P_h u, \chi_h) + r_h(\Pi_0^K u_h; u_h, \chi_h) - r_h(u; P_h u, \chi_h) \\ &= m_h((P_h u)_t, \chi_h) - (u_t, \chi_h) + \alpha(\rho, \chi_h) \\ &\quad + r_h(\Pi_0^K u_h; u_h, \chi_h) - r_h(u; P_h u, \chi_h). \end{aligned}$$

Following the same method used in [38], combined with polynomial consistency from Lemma 3.10, it follows that

$$\begin{aligned} |m_h((P_h u)_t, \chi_h) - (u_t, \chi_h)| &= \left| \sum_{K \in \mathcal{T}_h} m_h^K((P_h u)_t, \chi_h) - (u_t, \chi_h)_K \right| \\ &= \left| \sum_{K \in \mathcal{T}_h} m_h^K((P_h u)_t - \mathcal{P}_K^\ell u_t, \chi_h) - (u_t - \mathcal{P}_K^\ell u_t, \chi_h)_K \right| \\ &\lesssim \sum_{K \in \mathcal{T}_h} \|(P_h u)_t - \mathcal{P}_K^\ell u_t\|_{0,K} \|\chi_h\|_{0,K} + \|u_t - \mathcal{P}_K^\ell u_t\|_{0,K} \|\chi_h\|_{0,K}. \end{aligned}$$

Where we have used stability of the bilinear form (Lemma 3.11) in the last step. We now use Lemma 4.3 and properties of the L^2 projection detailed in Theorem 2.3, to show that

$$|m_h((P_h u)_t, \chi_h) - (u_t, \chi_h)| \lesssim h^\ell \|\chi_h\|_{0,h}.$$

Now, we take $\chi_h = \theta$ in (4.23) and see that

$$\begin{aligned} m_h(\theta_t, \theta) + \varepsilon^2 a_h(\theta, \theta) &= m_h((P_h u)_t, \theta) - (u_t, \theta) + \alpha(\rho, \theta) \\ &\quad + r_h(\Pi_0^K u_h; u_h, \theta) - r_h(u; P_h u, \theta). \end{aligned}$$

Using stability properties of the discrete forms alongside Lemmas 4.3 and 4.7, it holds that

$$\begin{aligned} \frac{1}{2} \frac{d}{dt} \|\theta\|_{0,h}^2 + \varepsilon^2 |\theta|_{2,h}^2 &\lesssim (h^\ell + \alpha \|\rho\|_{0,h}) \|\theta\|_{0,h} + |r_h(\Pi_0^K u_h; u_h, \theta) - r_h(u; P_h u, \theta)| \\ &\lesssim h^\ell \|\theta\|_{0,h} + (\|\theta\|_{0,h} + h^\ell) |\theta|_{1,h}. \end{aligned}$$

After an application of Young's inequality, we get the following

$$\lesssim h^{2\ell} + \|\theta\|_{0,h}^2 + |\theta|_{1,h}^2.$$

In order to conclude the proof, we observe that for any $v_h \in V_{h,\ell}$ and $0 < \gamma \leq \frac{1}{2}$, we can use an application of integration by parts, Cauchy-Schwarz, and Lemma 4.8, to show the following holds

$$|v_h|_{1,K}^2 = - \int_K \Delta v_h v_h \, dx + \int_{\partial K} v_h \partial_n v_h \, ds \lesssim \gamma \|\Delta v_h\|_{0,K}^2 + C_\gamma \|v_h\|_{0,K}^2 + h |v_h|_{2,K}^2.$$

Therefore $|\theta|_{1,h}^2 \lesssim (\gamma + h) |\theta|_{2,h}^2 + C_\gamma \|\theta\|_{0,h}^2$, hence

$$\frac{1}{2} \frac{d}{dt} \|\theta\|_{0,h}^2 + \varepsilon^2 |\theta|_{2,h}^2 \lesssim h^{2\ell} + \|\theta\|_{0,h}^2 + (\gamma + h) |\theta|_{2,h}^2 + C_\gamma \|\theta\|_{0,h}^2.$$

Therefore equation (4.21) follows from an application of Gronwall's lemma. \square

5. Numerical Results. In this section we present a fully discrete scheme and investigate the behaviour. The fully discrete scheme couples the VEM spatial discretization with a Runge-Kutta (RK) scheme, which combines a convex splitting (CS) method with a multi-stage additive RK method. For the method we use a nonlinear convex splitting of the energy $E(u)$, defined in (2.2), see e.g. [27, 28, 32, 35], where we split the energy into a contractive and expansive part as follows

$$E(u) = E_c(u) - E_e(u) = \int_{\Omega} \left(\frac{u^4}{4} + \frac{1}{4} + \frac{\varepsilon^2}{2} |\nabla u|^2 \right) dx - \int_{\Omega} \frac{u^2}{2} dx,$$

where $E_c(u)$ is treated implicitly, whereas $E_e(u)$ is treated explicitly. It is straightforward to show that $E_c(u)$ and $E_e(u)$ are both convex.

To introduce the fully discrete problem we split the interval $[0, T]$ into uniform subintervals and search for the solution at time t_n , $u_{h\tau}^n \in V_{h,\ell}$. We first split the semi-linear form r_h according to the convex splitting above, recalling that $\phi'(w) = 3w^2 - 1$,

$$\begin{aligned} r_{h,c}(\Pi_0^K u_h; v_h, w_h) - r_{h,e}(\Pi_0^K u_h; v_h, w_h) \\ = \sum_{K \in \mathcal{T}_h} \int_K 3(\Pi_0^K u_h)^2 \Pi_1^K v_h \cdot \Pi_1^K w_h \, dx - \sum_{K \in \mathcal{T}_h} \int_K \Pi_1^K v_h \cdot \Pi_1^K w_h \, dx \end{aligned}$$

for $u_h, v_h, w_h \in V_{h,\ell}$. We denote two RK methods using standard Butcher notation

$$(5.1) \quad \begin{array}{c|c} c & A \\ \hline & \hat{b}^T \end{array} = \begin{array}{c|ccc} c_1 & a_{11} & \cdots & a_{1s} \\ \vdots & \vdots & \ddots & \vdots \\ c_s & a_{s1} & \cdots & a_{ss} \\ \hline & \hat{b}_1 & \cdots & \hat{b}_s \end{array}, \quad \begin{array}{c|c} \hat{c} & \hat{A} \\ \hline & \hat{\hat{b}}^T \end{array} = \begin{array}{c|ccc} \hat{c}_1 & \hat{a}_{11} & \cdots & \hat{a}_{1s} \\ \vdots & \vdots & \ddots & \vdots \\ \hat{c}_s & \hat{a}_{s1} & \cdots & \hat{a}_{ss} \\ \hline & \hat{\hat{b}}_1 & \cdots & \hat{\hat{b}}_s \end{array}$$

for $A, \hat{A} \in \mathbb{R}^{s \times s}$, $b, \hat{b} \in \mathbb{R}^s$ and the coefficients $c, \hat{c} \in \mathbb{R}^s$ are given by $c = A1, \hat{c} = \hat{A}1$. Our fully discrete scheme is therefore given by

$$m_h(u_{h\tau}^{n+1} - u_{h\tau}^n, v_h) + \tau \sum_{i=1}^s b_i \left(\varepsilon^2 a_h(U^i, v_h) + r_{h,c}(U^i, U^i, v_h) \right) - \hat{b}_i r_{h,e}(U^i, U^i, v_h) = 0$$

for all $v_h \in V_{h,\ell}$, where the i -th stage is defined by

$$m_h(U^i - u_{h\tau}^n, v_h) + \tau \sum_{j=1}^s a_{ij} \left(\varepsilon^2 a_h(U^j, v_h) + r_{h,c}(U^j, U^j, v_h) \right) - \hat{a}_{ij} r_{h,e}(U^j, U^j, v_h) = 0$$

for all $v_h \in V_{h,\ell}$, for $i = 1, \dots, s$.

The first scheme we use is the simple first order CS “Forward-Backward Euler” method (CSRK-1) [35], with Butcher notation

$$(5.2) \quad \begin{array}{c|ccc} c & A & & \\ \hline & b^T & & \end{array} = \begin{array}{c|ccc} & 0 & 0 & \\ \hline & 1 & 0 & 1 \\ & & 0 & 1 \end{array}, \quad \begin{array}{c|ccc} \hat{c} & \hat{A} & & \\ \hline & \hat{b}^T & & \end{array} = \begin{array}{c|ccc} & 0 & 0 & 0 \\ \hline & 1 & 1 & 0 \\ & & 1 & 0 \end{array}.$$

The other method we consider is the second order CS Runge-Kutta method (CSRK-2) presented in [32], rewritten in Butcher notation as

$$(5.3) \quad \begin{array}{c|ccccc} c & A & & & \\ \hline & b^T & & & \end{array} = \begin{array}{c|ccccc} & 0 & 0 & 0 & 0 & \\ \hline & 1 & 0 & 1 & 0 & 0 \\ & \frac{3}{2} & 0 & \frac{1}{2} & 1 & 0 \\ & 1 & 0 & 1 & -1 & 1 \\ \hline & & 0 & 1 & -1 & 1 \end{array}, \quad \begin{array}{c|ccccc} \hat{c} & \hat{A} & & & \\ \hline & \hat{b}^T & & & \end{array} = \begin{array}{c|ccccc} & 0 & 0 & 0 & 0 & \\ \hline & 1 & 1 & 0 & 0 & 0 \\ & \frac{3}{2} & \frac{1}{2} & 1 & 0 & 0 \\ & 1 & 1 & -1 & 1 & 0 \\ \hline & & 1 & -1 & 1 & 0 \end{array}.$$

The schemes defined in both (5.2) and (5.3) are shown to be energy stable [32, 35].

The code we use to carry out the simulations is based on the Distributed and Unified Numerics Environment (DUNE) software framework [6] and implemented within the DUNE-FEM module [18]. DUNE is open source software implemented in C++, but since a user has access to a Python frontend [19], they can easily perform numerical experiments by describing mathematical models using the domain specific form language UFL [2]. Tutorials including some VEM examples can be found in [17].

5.1. Test 1: General convergence. In this section we investigate convergence to an exact solution. In this test we reduce τ alongside h , starting with $\tau = 10^{-2}$. We fix $\varepsilon = 1/10$ for these experiments and run them on both a structured simplex grid consisting of half square triangles and a Voronoi grid discretizing the unit square. The L^2 , H^1 , and H^2 errors are computed at every time step and we present the maximum errors in each case. We set the forcing f so that the exact solution is given by

$$u(x, y, t) = \sin(2\pi t) \cos(2\pi x) \cos(2\pi y).$$

We investigate the convergence for polynomial orders $\ell = 2, 4$ for both the CSRK-1 (5.2) and CSRK-2 (5.3) time stepping methods. The results on the simplex grid are shown in Table 1 and the results on a Voronoi polygonal grid are shown in Table 2.

The results from this convergence test are in line with expectations. Since the CSRK-1 method is first order accurate in time and the CSRK-2 method is second order accurate, when combining one of these methods with the order ℓ VEM method, we should expect to see L^2 convergence rates of order $\min\{\ell, n\}$ where $n \in \{1, 2\}$ is the order from the CSRK- n method. In order to see the optimal L^2 convergence $O(h^\ell)$ (Theorem 4.9), we look at the $\ell = 2$ VEM method coupled with the CSRK-2 time stepping. These results are shown in Tables 1b, 2b. Note that the convergence rates in the H^1 and H^2 norms are also what we would expect to see if we extended Theorem 4.9 to include convergence results in both H^1 and H^2 norms according to classic FE theory. For example, the rate for the H^2 error with $\ell = 2$ is equal to 1 while the higher order is clearly visible in the $\ell = 4$, CSRK-2 results (Tables 1c, 2c).

TABLE 1

Test 1: L^2 , H^1 , and H^2 errors and convergence rates for the convergence test on a structured simplex grid.

(a) Test 1: convergence test with CSRK-1 time stepping and polynomial order $\ell = 2$.

size	dofs	h	L^2 -error	L^2 -eoc	H^1 -error	H^1 -eoc	H^2 -error	H^2 -eoc
50	121	0.2828	1.9412e-01	—	1.8409e+00	—	1.8815e+01	—
200	441	0.1414	9.1284e-02	1.09	8.5348e-01	1.11	8.9738e+00	1.07
800	1681	0.0707	4.5175e-02	1.01	4.1419e-01	1.04	4.3675e+00	1.04
3200	6561	0.0354	2.2522e-02	1.0	2.0391e-01	1.02	2.1492e+00	1.02

(b) Test 1: convergence test with CSRK-2 time stepping and polynomial order $\ell = 2$.

size	dofs	h	L^2 -error	L^2 -eoc	H^1 -error	H^1 -eoc	H^2 -error	H^2 -eoc
50	121	0.2828	1.1203e-01	—	1.1001e+00	—	1.6705e+01	—
200	441	0.1414	2.9845e-02	1.91	3.0147e-01	1.87	8.0622e+00	1.05
800	1681	0.0707	7.3555e-03	2.02	7.6541e-02	1.98	3.9588e+00	1.03
3200	6561	0.0354	1.7710e-03	2.05	1.8949e-02	2.01	1.9692e+00	1.01

(c) Test 1: convergence test with CSRK-2 time stepping and polynomial order $\ell = 4$.

size	dofs	h	L^2 -error	L^2 -eoc	H^1 -error	H^1 -eoc	H^2 -error	H^2 -eoc
50	511	0.2828	2.2046e-02	—	1.9803e-01	—	1.8769e+00	—
200	1921	0.1414	5.5596e-03	1.99	5.0125e-02	1.98	4.8603e-01	1.95
800	7441	0.0707	1.0552e-03	2.4	9.7040e-03	2.37	1.0401e-01	2.22
3200	29281	0.0354	1.6197e-04	2.7	1.6259e-03	2.58	2.6636e-02	1.97

TABLE 2

Test 1: L^2 , H^1 , and H^2 errors and convergence rates for the convergence test on a Voronoi polygonal grid.

(a) Test 1: convergence test with CSRK-1 time stepping and polynomial order $\ell = 2$.

size	dofs	h	L^2 -error	L^2 -eoc	H^1 -error	H^1 -eoc	H^2 -error	H^2 -eoc
25	128	0.3288	2.5850e-01	—	2.3431e+00	—	2.2020e+01	—
100	503	0.1535	1.1302e-01	1.09	1.0281e+00	1.08	1.0548e+01	0.97
400	2003	0.0751	5.1155e-02	1.11	4.5992e-01	1.13	4.9724e+00	1.05
1600	8003	0.0402	2.3960e-02	1.21	2.1488e-01	1.22	2.4843e+00	1.11

(b) Test 1: convergence test with CSRK-2 time stepping and polynomial order $\ell = 2$.

size	dofs	h	L^2 -error	L^2 -eoc	H^1 -error	H^1 -eoc	H^2 -error	H^2 -eoc
25	128	0.3288	1.9833e-01	—	1.7472e+00	—	2.0820e+01	—
100	503	0.1535	4.6127e-02	1.92	4.5037e-01	1.78	9.9688e+00	0.97
400	2003	0.0751	1.0867e-02	2.02	1.0755e-01	2.0	4.9206e+00	0.99
1600	8003	0.0402	2.5869e-03	2.29	2.5990e-02	2.27	2.4679e+00	1.1

(c) Test 1: convergence test with CSRK-2 time stepping and polynomial order $\ell = 4$.

size	dofs	h	L^2 -error	L^2 -eoc	H^1 -error	H^1 -eoc	H^2 -error	H^2 -eoc
25	457	0.3288	2.2198e-02	—	1.9974e-01	—	1.9335e+00	—
100	1807	0.1535	5.5609e-03	1.82	5.0147e-02	1.81	4.8954e-01	1.8
400	7207	0.0751	1.0552e-03	2.33	9.7041e-03	2.3	1.0424e-01	2.16
1600	28807	0.0402	1.6145e-04	3.0	1.6223e-03	2.86	2.6661e-02	2.18

5.2. Test 2: Evolution of a cross. As considered in e.g. [3, 13, 34], for this experiment we monitor the evolution of initial data relating to a cross-shaped interface between phases. The initial data is described as follows.

$$u_0(x) = \begin{cases} 0.95 & \text{if } |(y - \frac{1}{2}) - \frac{2}{5}(x - \frac{1}{2})| + |\frac{2}{5}(x - \frac{1}{2}) + (y - \frac{1}{2})| < \frac{1}{5}, \\ 0.95 & \text{if } |(x - \frac{1}{2}) - \frac{2}{5}(y - \frac{1}{2})| + |\frac{2}{5}(y - \frac{1}{2}) + (x - \frac{1}{2})| < \frac{1}{5}, \\ -0.95 & \text{otherwise.} \end{cases}$$

We carry out this experiment on the unit square using the same two different meshes as in Section 5.1, the structured simplex mesh and the Voronoi polygonal mesh. We also take multiple values for the interface parameter: $\varepsilon = 1/100, 1/50$, and $1/25$ and investigate their behaviour. We fix $\tau = 10^{-3}$, use the CSRK-2 time stepping method (5.3) for these simulations and run the test to time $T = 0.8$. We look at five different combinations of polynomial order ℓ and grid size N for this test. These combinations are detailed in Table 3 alongside the total number of dofs for each of these combinations on both meshes we consider.

TABLE 3

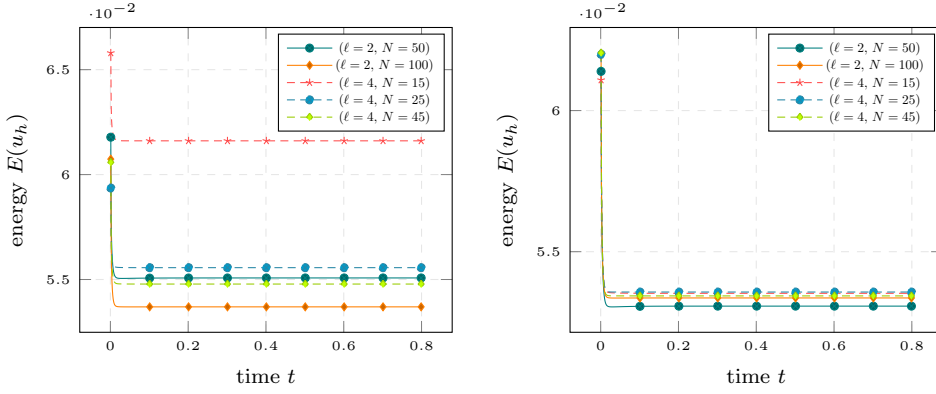
Combinations of polynomial order and grid N showing the size (total number of polygons), grid size h , and number of dofs for each combination on both the structured simplex mesh and the Voronoi polygonal mesh.

order	grid N	simplex mesh			Voronoi mesh		
		size	h	dofs	size	h	dofs
$\ell = 2$	50	5000	0.0283	10201	2500	0.0326	12503
$\ell = 2$	100	20000	0.0141	40401	10000	0.0169	50003
$\ell = 4$	15	450	0.0943	4231	225	0.1008	4057
$\ell = 4$	25	1250	0.0566	11551	625	0.0676	11257
$\ell = 4$	45	4050	0.0314	36991	2025	0.0373	36457

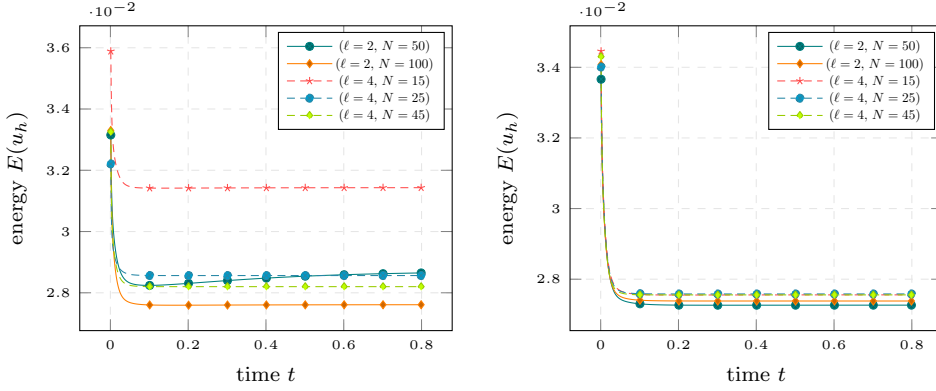
Figure 3 shows the evolution at the end time frame for both $\varepsilon = 1/25, 1/100$ on the simplex mesh and Voronoi mesh, with the grids overlaid in the last two columns. We can see from Figure 3 that in most cases the initial data evolves to a circular interface. Observe from Figures 3a and 3b that for $\ell = 2$ the initial data evolves to a rotated ellipse on the simplex mesh but still evolves to a circular steady state if we use a larger interface parameter ($\varepsilon = 1/25$). Also notice that due to the isotropy of the Voronoi polygonal mesh, this problem is avoided completely for $\ell = 2$ on this grid. We also point out that using the same number of dofs as with $\ell = 2$ but with $\ell = 4$ on much coarser grids, leads to improved results and the ellipse problem seen for the simplex mesh in Figures 3a and 3b is avoided altogether (see Figures 3c, 3d, and 3e).

The energy decay for this problem is shown in Figure 2 and as expected the energy decreases in nearly all cases. At each time step we compute the energy $E(u_h)$ (2.2) of the discrete solution u_h . We included in this test a stopping criteria which meant that the experiment terminates if the energy increased by more than 10% of the minimum energy, therefore we see in Figure 2c only half the energy values plotted for the ($\ell = 2$, $N = 50$) method. In this instance, the energy began to increase by more than 10%, due to the initial data evolving to a rotated ellipse shape on this mesh. We see the same phenomenon happening for $\ell = 2$ on the finer $N = 100$ grid but the energy only starting to increase later on in time, and from Figure 3b we see a less harsh ellipse shape than in Figure 3a.

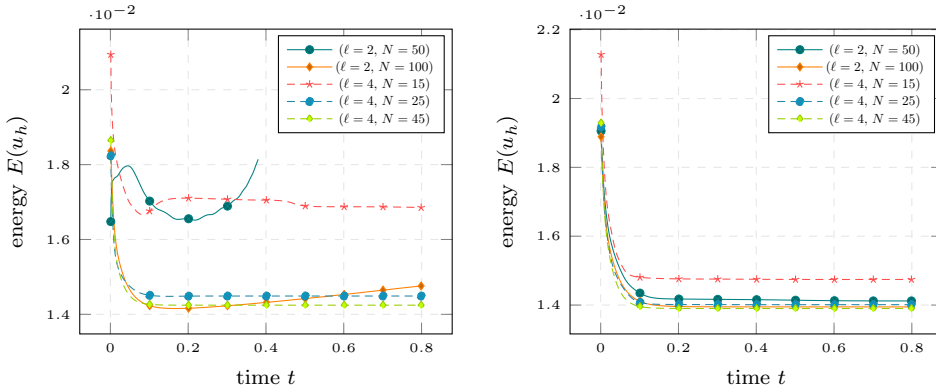
We also show the evolution for the $\ell = 4$ method with the $N = 25$ grids for two epsilon values ($\varepsilon = 1/25, 1/100$) in Figure 4 at four different time frames.



(a) Energy plots for $\varepsilon = 1/25$ on the structured simplex mesh (left) and Voronoi polygonal mesh (right).

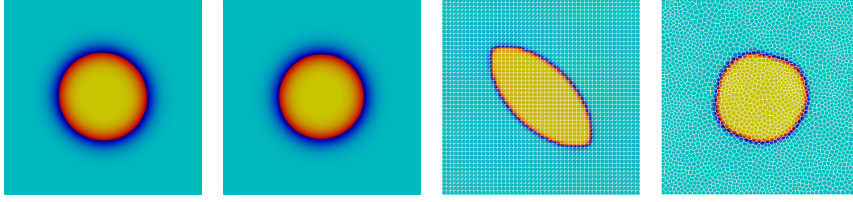


(b) Energy plots for $\varepsilon = 1/50$ on the structured simplex mesh (left) and Voronoi polygonal mesh (right).

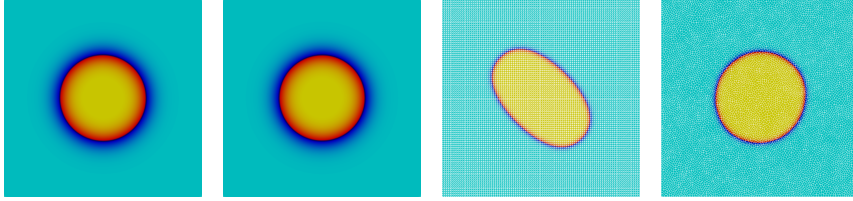


(c) Energy plots for $\varepsilon = 1/100$ on the structured simplex mesh (left) and Voronoi polygonal mesh (right). Notice that the $(\ell = 2, N = 50)$ test was terminated on the simplex mesh (left) as the energy started increasing, as seen here.

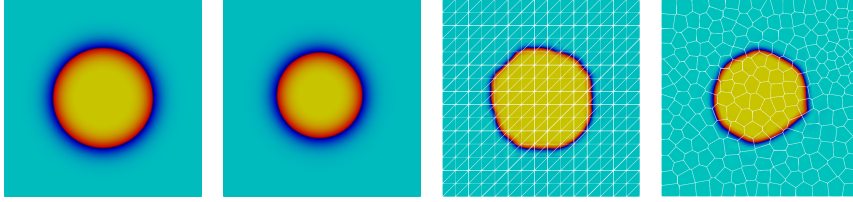
FIG. 2. Test 2: energy decay plots (energy $E(u_h)$ vs time t) for the cross evolution problem.



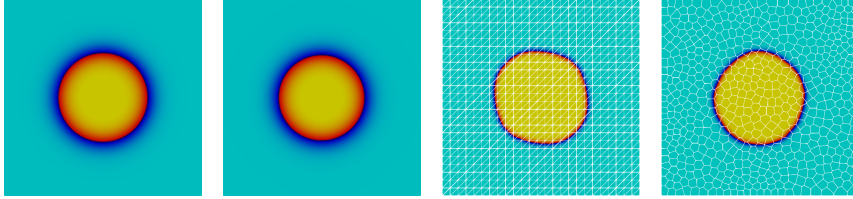
(a) Polynomial order $\ell = 2$ on the $N = 50$ grids. Note that the $(\ell = 2, N = 50)$ method on the simplex mesh with $\varepsilon = 1/100$ (third image in this row) is shown only at time frame $t = 0.4$ since the energy in this case started increasing (see Figure 2).



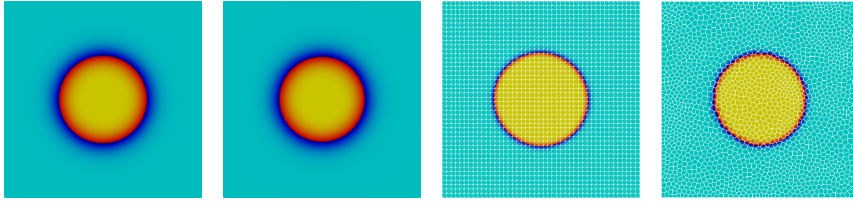
(b) Polynomial order $\ell = 2$ on the $N = 100$ grids.



(c) Polynomial order $\ell = 4$ on the $N = 15$ grids.



(d) Polynomial order $\ell = 4$ on the $N = 25$ grids.



(e) Polynomial order $\ell = 4$ on the $N = 45$ grids.

FIG. 3. Test 2: evolution of a cross displayed at the time frame $t = 0.8$. The first two columns correspond to $\varepsilon = 1/25$ on the simplex mesh and the Voronoi polygonal mesh respectively. The last two columns correspond to $\varepsilon = 1/100$ on the simplex mesh and the Voronoi polygonal mesh respectively. Details of the number of elements and dofs in the meshes can be found in Table 3.

5.3. Test 3: Spinodal decomposition. For this final experiment we turn our attention to the spinodal decomposition of a binary mixture. To model this phenomenon we choose the initial data u_0 to be a random perturbation between -1 and 1 located in a circle of diameter 0.3 in the centre of the domain. We take the interface parameter to be $\varepsilon = 1/100$, with time step $\tau = 10^{-2}$, and we use the CSRK-2 time stepping method (5.3). Snapshots of the results on both the structured simplex grid and the Voronoi polygonal mesh are shown in Figure 5. We only present the results from this test for $\ell = 4$ but note that the results for lower orders ($\ell = 2, 3$) were analogous. Note that the random initial conditions used for the two grids are different and result in the difference in the end configurations seen in Figure 5.

6. Conclusion. In this paper we have developed a fully nonconforming virtual element method of arbitrary approximation order for the discretization of the two dimensional Cahn-Hilliard equation. We have applied the projection approach taken in [16] to the fourth-order nonlinear Cahn-Hilliard problem and were able to define the discrete forms directly without using an averaging technique for the nonlinear term, as seen in [3]. This approach enabled us to prove optimal order error estimates in L^2 for the continuous-in-time (semidiscrete) scheme. The VEM spatial discretization was coupled with a convex splitting Runge-Kutta (CSRK) method to create a fully discrete scheme and the behaviour investigated with numerical experiments. The theoretical convergence result was verified numerically and standard benchmark tests from the literature were carried out.

Appendix A. Proof of technical results. We dedicate this section to the proof of some technical lemmas necessary for the error analysis. Firstly, we give the proof of Lemma 4.4.

Proof of Lemma 4.4. We begin by introducing the interpolation $I_h z$ of z into our nonconforming VEM space $V_{h,\ell}$,

$$|b(u - P_h u, z)| = |b(u - P_h u, z - I_h z) + b(u - P_h u, I_h z)|.$$

The first term can be bounded easily using the continuity of the bilinear form $b(\cdot, \cdot)$, (4.6), and interpolation properties of I_h (3.6). Hence, we can show that

$$|b(u - P_h u, z - I_h z)| \leq \|u - P_h u\|_{2,h} \|z - I_h z\|_{2,h} \lesssim h^\ell \|u - P_h u\|_{1,h}.$$

We rewrite the remaining term using $z_h := I_h z - z$, and see that

$$b(u - P_h u, I_h z) = b(u, z_h) + b(u, z) - b(P_h u, I_h z).$$

The continuous solution u satisfies

$$b(u, z) = \varepsilon^2 a(u, z) + r(u; u, z) + \alpha(u, z) = (\varepsilon^2 \Delta^2 u - \nabla \cdot (\phi'(u) \nabla u) + \alpha u, z)$$

and using (4.4) as well as the definition of the elliptic projection in (4.2), it follows that

$$\begin{aligned} b(u, z_h) + b(u, z) &= \varepsilon^2 a(u, z_h) + r(u; u, z_h) + \alpha(u, z_h) + b(u, z) \\ &= (\varepsilon^2 \Delta^2 u - \nabla \cdot (\phi'(u) \nabla u) + \alpha u, z_h + z) + \mathcal{N}(u, z_h) \\ &= b_h(P_h u, I_h z) + \mathcal{N}(u, z_h) \end{aligned}$$

where $\mathcal{N}(u, z_h)$ is defined in (4.5). Noting that, by definition

$$b_h(P_h u, I_h z) = b(P_h u, I_h z) + \varepsilon^2 (a_h(P_h u, I_h z) - a(P_h u, I_h z))$$

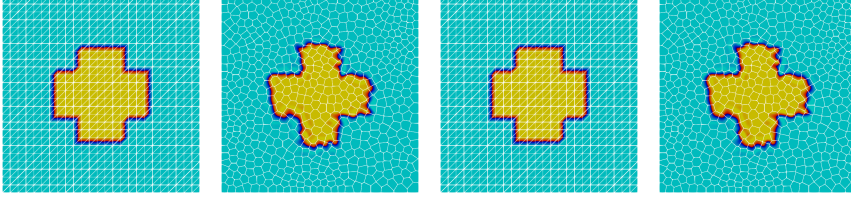
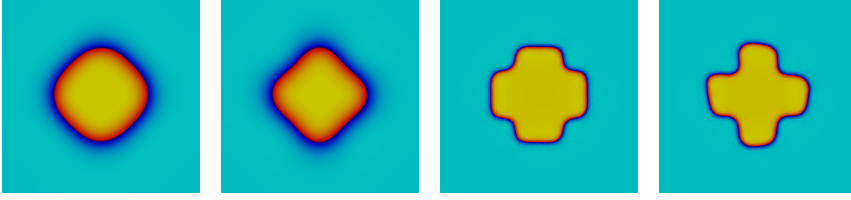
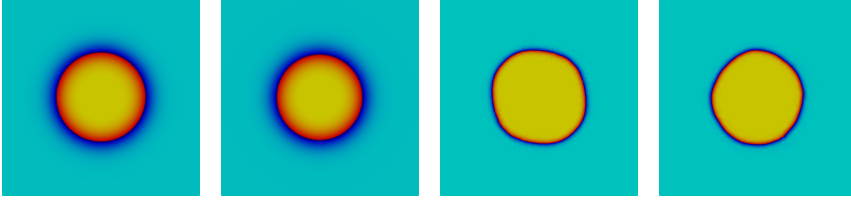
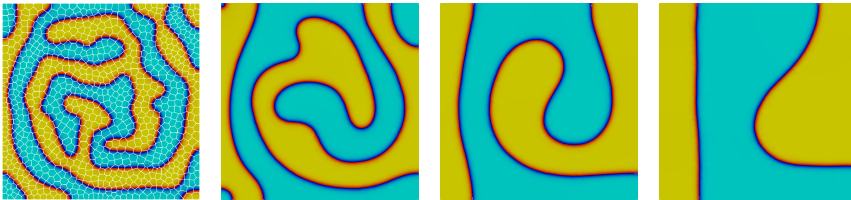
(a) Evolution of a cross at time $t = 0$ with order $\ell = 4$ on the $N = 25$ grids.(b) Evolution of a cross at time $t = 0.004$.(c) Evolution of a cross at time $t = 0.8$.

FIG. 4. *Test 2: evolution of a cross for order $\ell = 4$ on the $N = 25$ grids displayed at three different time frames from top to bottom ($t = 0, 0.004, 0.8$). The first two columns correspond to $\varepsilon = 1/25$ on the structured simplex mesh and the Voronoi polygonal mesh respectively. The last two columns correspond to $\varepsilon = 1/100$ on the structured simplex mesh and the Voronoi polygonal mesh respectively.*



(a) Structured simplex mesh consisting of 2048 elements (18817 dof).



(b) Voronoi polygonal mesh consisting of 1024 elements (18439 dof).

FIG. 5. *Test 3: spinodal decomposition with order $\ell = 4$ displayed at four time frames from left to right ($t = 0.04, 0.4, 1.6, 5$). Notice that the visible differences in the images is due to the difference in the starting configurations from different initial random conditions.*

$$+ r_h(u; P_h u, I_h z) - r(u; P_h u, I_h z).$$

So we observe that

$$\begin{aligned} |b(u - P_h u, I_h z)| &= |b(u, z_h) + b(u, z) - b(P_h u, I_h z) - b_h(P_h u, I_h z) + b_h(P_h u, I_h z)| \\ &\leq |\mathcal{N}(u, z_h)| + \varepsilon^2 |a_h(P_h u, I_h z) - a(P_h u, I_h z)| \\ &\quad + |r_h(u; P_h u, I_h z) - r(u; P_h u, I_h z)| \\ &= T_1 + T_2 + T_3. \end{aligned}$$

For T_1 we apply Lemma 4.2 and (4.11) to see that

$$(A.1) \quad T_1 \lesssim h^{\ell-1} |z - I_h z|_{2,h} \lesssim h^\ell \|z\|_{3,\Omega} \lesssim h^\ell \|u - P_h u\|_{1,h}.$$

For the second term T_2 , we introduce the L^2 projection of z , as well as the L^2 projection of u , and use polynomial consistency from Lemma 3.10.

$$\begin{aligned} T_2 &= \varepsilon^2 |a_h(P_h u, I_h z) - a(P_h u, I_h z)| \\ &= \varepsilon^2 \left| \sum_{K \in \mathcal{T}_h} a_h^K(I_h z - \mathcal{P}_\ell^K z, P_h u - \mathcal{P}_\ell^K u) - a^K(I_h z - \mathcal{P}_\ell^K z, P_h u - \mathcal{P}_\ell^K u) \right| \\ (A.2) \quad &\lesssim \varepsilon^2 |I_h z - \mathcal{P}_\ell^K z|_{2,h} |P_h u - \mathcal{P}_\ell^K u|_{2,h} \lesssim h \|z\|_{3,\Omega} h^{\ell-1} \lesssim h^\ell \|u - P_h u\|_{1,h}. \end{aligned}$$

For the final term, T_3 , we note that due to the fact that the gradient projection is exact for polynomials, it holds that $r_h(u; \mathcal{P}_\ell^K u, \mathcal{P}_\ell^K z) = r(u; \mathcal{P}_\ell^K u, \mathcal{P}_\ell^K z)$. Therefore,

$$\begin{aligned} T_3 &= |r_h(u; P_h u, I_h z) - r(u; P_h u, I_h z)| \\ &= |r_h(u; P_h u - \mathcal{P}_\ell^K u, I_h z - \mathcal{P}_\ell^K z) + r_h(u; \mathcal{P}_\ell^K u, I_h z) + r_h(u; P_h u, \mathcal{P}_\ell^K z) \\ &\quad - r_h(u; \mathcal{P}_\ell^K u, \mathcal{P}_\ell^K z) + r(u; \mathcal{P}_\ell^K u, \mathcal{P}_\ell^K z) \\ &\quad - r(u; P_h u - \mathcal{P}_\ell^K u, I_h z - \mathcal{P}_\ell^K z) - r(u; \mathcal{P}_\ell^K u, I_h z) - r(u; P_h u, \mathcal{P}_\ell^K z)| \\ (A.3) \quad &\leq |r_h(u; P_h u - \mathcal{P}_\ell^K u, I_h z - \mathcal{P}_\ell^K z) - r(u; P_h u - \mathcal{P}_\ell^K u, I_h z - \mathcal{P}_\ell^K z)| \\ (A.4) \quad &+ |r_h(u; \mathcal{P}_\ell^K u, I_h z) - r(u; \mathcal{P}_\ell^K u, I_h z)| \\ (A.5) \quad &+ |r_h(u; P_h u, \mathcal{P}_\ell^K z) - r(u; P_h u, \mathcal{P}_\ell^K z)|. \end{aligned}$$

The first term (A.3) can be treated in the same way as T_2 and we can show that

$$\begin{aligned} &|r_h(u; P_h u - \mathcal{P}_\ell^K u, I_h z - \mathcal{P}_\ell^K z) - r(u; P_h u - \mathcal{P}_\ell^K u, I_h z - \mathcal{P}_\ell^K z)| \\ &\lesssim \|\phi'(u)\|_{L^\infty} |P_h u - \mathcal{P}_\ell^K u|_{1,h} |I_h z - \mathcal{P}_\ell^K z|_{1,h} \\ (A.6) \quad &\lesssim h^\ell \|u - P_h u\|_{1,h}. \end{aligned}$$

For the next term (A.4), since $\mathcal{P}_\ell^K u \in \mathbb{P}_\ell(K)$, the stabilization part of r_h vanishes and so we have the following

$$\begin{aligned} &|r_h(u; \mathcal{P}_\ell^K u, I_h z) - r(u; \mathcal{P}_\ell^K u, I_h z)| \\ &= \left| \sum_{K \in \mathcal{T}_h} \int_K \phi'(u) (\mathcal{P}_{\ell-1}^K (\nabla \mathcal{P}_\ell^K u) \cdot \mathcal{P}_{\ell-1}^K \nabla I_h z - \nabla \mathcal{P}_\ell^K u \cdot \nabla I_h z) \, dx \right| \\ &= \left| \sum_{K \in \mathcal{T}_h} \int_K \phi'(u) (\nabla \mathcal{P}_\ell^K u) \cdot (\mathcal{P}_{\ell-1}^K - I) \nabla I_h z \, dx \right|. \end{aligned}$$

$$\begin{aligned}
&= \left| \sum_{K \in \mathcal{T}_h} \int_K (\mathcal{P}_{\ell-1}^K - I)(\phi'(u) \nabla \mathcal{P}_\ell^K u) \cdot (\nabla I_h z - \mathcal{P}_0^K z) \, dx \right| \\
&\leq \sum_{K \in \mathcal{T}_h} \|(\mathcal{P}_{\ell-1}^K - I)\phi'(u) \nabla \mathcal{P}_\ell^K u\|_{0,K} \|\nabla I_h z - \mathcal{P}_0^K z\|_{0,K} \\
(A.7) \quad &\lesssim h^{\ell-1} h \|z\|_{3,\Omega} \lesssim h^\ell \|u - P_h u\|_{1,h}.
\end{aligned}$$

For the final term in T_3 , (A.5), we again note that since $\mathcal{P}_\ell^K z \in \mathbb{P}_\ell(K)$, the stabilization part of r_h vanishes, and so

$$\begin{aligned}
&|r_h(u; P_h u, \mathcal{P}_\ell^K z) - r(u; P_h u, \mathcal{P}_\ell^K z)| \\
&= \left| \sum_{K \in \mathcal{T}_h} \int_K \phi'(u) (\mathcal{P}_{\ell-1}^K \nabla P_h u \cdot \mathcal{P}_{\ell-1}^K \nabla \mathcal{P}_\ell^K z - \nabla P_h u \cdot \mathcal{P}_\ell^K z) \, dx \right| \\
&= \left| \sum_{K \in \mathcal{T}_h} \int_K \phi'(u) (\mathcal{P}_{\ell-1}^K - I) \nabla P_h u \cdot (\nabla \mathcal{P}_\ell^K z) \, dx \right| \\
&= \left| \sum_{K \in \mathcal{T}_h} \int_K \phi'(u) ((I - \mathcal{P}_{\ell-1}^K)(\nabla u - \nabla P_h u) - (I - \mathcal{P}_{\ell-1}^K) \nabla u) \cdot (\nabla \mathcal{P}_\ell^K z) \, dx \right| \\
&\leq \sum_{K \in \mathcal{T}_h} \|\phi'(u)\|_{L^\infty} h^1 |\nabla u - \nabla P_h u|_{1,K} \|\nabla \mathcal{P}_\ell^K z\|_{0,K} \\
&\quad + \sum_{K \in \mathcal{T}_h} \|\phi'(u)\|_{L^\infty} h^{\ell-1+1} |\nabla u|_{\ell,K} \|\nabla \mathcal{P}_\ell^K z\|_{0,K} \\
(A.8) \quad &\lesssim h^\ell \|u - P_h u\|_{1,h}
\end{aligned}$$

where we have used (4.6), (4.11), and stability of the L^2 projection in the last step. Hence, by combining the estimates from (A.1), (A.2), (A.6), (A.7), and (A.8), it holds that

$$|b(u - P_h u, I_h z)| \leq T_1 + T_2 + T_3 \lesssim h^\ell \|u - P_h u\|_{1,h}.$$

This concludes the proof. \square

Next, we give the proof of Lemma 4.5, necessary for the proof of the estimates (4.9)-(4.8) in Lemma 4.3.

Proof of Lemma 4.5. Using Lemma 3.7, since $P_h u, \eta_h \in V_{h,\ell}$, we can show the following

$$\begin{aligned}
&|(\phi''(u) u_t \Pi_1^K P_h u, \Pi_1^K \eta_h)_{0,h} - (\phi''(u) u_t \nabla u, \nabla \eta_h)_{0,h}| \\
&= \left| \sum_{K \in \mathcal{T}_h} \int_K \phi''(u) u_t (\mathcal{P}_{\ell-1}^K \nabla P_h u \cdot \mathcal{P}_{\ell-1}^K \nabla \eta_h - \nabla u \cdot \nabla \eta_h) \, dx \right| \\
&= \left| \sum_{K \in \mathcal{T}_h} \int_K (\mathcal{P}_{\ell-1}^K (\phi''(u) u_t \mathcal{P}_{\ell-1}^K \nabla P_h u) - \phi''(u) u_t \nabla u) \cdot \nabla \eta_h \, dx \right|
\end{aligned}$$

We now introduce the constant projection of the gradient of η_h , $\mathcal{P}_0^K(\nabla \eta_h)$ and see that

$$\leq \left| \sum_{K \in \mathcal{T}_h} \int_K (\mathcal{P}_{\ell-1}^K \{ \phi''(u) u_t \mathcal{P}_{\ell-1}^K \nabla P_h u - \phi''(u) u_t \mathcal{P}_{\ell-1}^K \nabla u \}) \cdot \nabla \eta_h \, dx \right|$$

$$\begin{aligned}
& + \left| \sum_{K \in \mathcal{T}_h} \int_K \left((\mathcal{P}_{\ell-1}^K - I)(\phi''(u)u_t \mathcal{P}_{\ell-1}^K \nabla u) \right) \cdot (\nabla \eta_h - \mathcal{P}_0^K(\nabla \eta_h)) \, dx \right| \\
& + \left| \sum_{K \in \mathcal{T}_h} \int_K \left(\phi''(u)u_t \mathcal{P}_{\ell-1}^K \nabla u - \phi''(u)u_t \nabla u \right) \cdot \nabla \eta_h \, dx \right| \\
& \leq \sum_{K \in \mathcal{T}_h} \|\phi''(u)u_t \mathcal{P}_{\ell-1}^K (\nabla P_h u - \nabla u)\|_{0,K} \|\nabla \eta_h\|_{0,K} \\
& \quad + \sum_{K \in \mathcal{T}_h} h^{\ell-1} |\phi''(u)u_t \mathcal{P}_{\ell-1}^K \nabla u|_{\ell-1} \|\nabla \eta_h - \mathcal{P}_0^K(\nabla \eta_h)\|_{0,K} \\
& \quad + \sum_{K \in \mathcal{T}_h} \|\phi''(u)u_t\|_{L^\infty} \|\mathcal{P}_{\ell-1}^K \nabla u - \nabla u\|_{0,K} \|\nabla \eta_h\|_{0,K} \\
& \lesssim h^\ell \|\eta_h\|_{2,h}
\end{aligned}$$

where we have used stability of the L^2 projection and (4.7). \square

Lastly, we give the proof of Lemma 4.8, which is necessary for the proof of L^2 convergence in Theorem 4.9.

Proof of Lemma 4.8. Recall that for any $w_h \in V_{h,\ell} \subset H_\ell^{2,nc}(\mathcal{T}_h)$, and for any edge $e \in \mathcal{E}_h$, the following properties hold,

$$(A.9) \quad \int_e [w_h] p \, ds = 0 \quad \forall p \in \mathbb{P}_{\ell-3}(e),$$

$$(A.10) \quad \int_e [\partial_n w_h] p \, ds = 0 \quad \forall p \in \mathbb{P}_{\ell-2}(e).$$

Observe that the following holds

$$\left| \sum_{K \in \mathcal{T}_h} \int_{\partial K} (\partial_n z_h) w_h \, ds \right| = \left| \sum_{e \in \mathcal{E}_h} \int_e (\{w_h\} [\partial_n z_h] + \{\partial_n z_h\} [w_h]) \, ds \right| \leq A_I + A_{II}$$

where we use $\{\cdot\}$ to denote the average of a function v , $\{v\} := \frac{1}{2}(v|_{K^+} + v|_{K^-})$ for any interior edge $e \subset \partial K^+ \cap \partial K^-$. For a boundary edge $e \in \mathcal{E}_h^{\text{bdry}}$ we define $\{v\} := v|_e$.

Using (A.10), for the first term A_I , it holds that

$$\begin{aligned}
A_I &= \left| \sum_{e \in \mathcal{E}_h} \int_e \{w_h\} [\partial_n z_h] \, ds \right| \leq \left| \sum_{e \in \mathcal{E}_h} \int_e (\{w_h\} - \mathcal{P}_0^e \{w_h\}) [\partial_n z_h] \, ds \right| \\
&\leq \left| \sum_{e \in \mathcal{E}_h} \int_e (\{w_h\} - \mathcal{P}_0^e \{w_h\}) ([\partial_n z_h] - \mathcal{P}_0^e [\partial_n z_h]) \, ds \right| \\
&\lesssim h^{1-\frac{1}{2}} |w_h|_{1,h} h^{1-\frac{1}{2}} |\partial_n z_h|_{1,h} \\
&\lesssim h |w_h|_{1,h} |z_h|_{2,h}.
\end{aligned}$$

For the second term A_{II} , we follow the method used in [4]. In view of assumption (A3), for each edge we define the linear Lagrange interpolant $I_{T(e)}^1$ of z_h on the sub-triangle $T(e)$, made from connecting the interior point x_K to the endpoints of the edge e . Since $z_h \in V_{h,\ell}$, it also satisfies $z_h \in H^2(K)$, and so we can build the interpolant by using the values at the vertices of $T(e)$. Further, z_h is continuous at the endpoints of e and so

$$[I_{T(e)}^1(w_h)]|_e = 0.$$

Therefore, by using standard interpolation estimates and a trace inequality, we see that

$$\begin{aligned} A_{II} &= \left| \sum_{e \in \mathcal{E}_h} \int_e \{\partial_n z_h\} [w_h] \, ds \right| = \left| \sum_{e \in \mathcal{E}_h} \int_e \{\partial_n z_h\} ([w_h] - [I_{T(e)}^1(w_h)]) \, ds \right| \\ &\lesssim h |z_h|_{2,h} |w_h|_{2,h}, \end{aligned}$$

hence (4.20) holds, as required. \square

Acknowledgements. The authors would like to acknowledge the University of Warwick Scientific Computing Research Technology Platform for assistance in the research described in this paper.

REFERENCES

- [1] B. AHMAD, A. ALSAEDI, F. BREZZI, L. MARINI, AND A. RUSSO, *Equivalent projectors for virtual element methods*, Comput. Math. Appl., 66 (2013), pp. 376–391, <https://doi.org/10.1016/j.camwa.2013.05.015>.
- [2] M. S. ALNÆS, A. LOGG, K. B. ØLGAARD, M. E. ROGNES, AND G. N. WELLS, *Unified form language: A domain-specific language for weak formulations of partial differential equations*, ACM Trans. Math. Softw., 40 (2014), <https://doi.org/10.1145/2566630>.
- [3] P. F. ANTONIETTI, L. BEIRÃO DA VEIGA, S. SCACCHI, AND M. VERANI, *A C^1 Virtual Element Method for the Cahn–Hilliard Equation with Polygonal Meshes*, SIAM J. Numer. Anal., 54 (2016), pp. 34–56, <https://doi.org/10.1137/15M1008117>.
- [4] P. F. ANTONIETTI, G. MANZINI, AND M. VERANI, *The fully nonconforming virtual element method for biharmonic problems*, Math. Models Methods Appl. Sci., 28 (2018), pp. 387–407, <https://doi.org/10.1142/S0218202518500100>.
- [5] P. F. ANTONIETTI, G. MANZINI, AND M. VERANI, *The conforming virtual element method for polyharmonic problems*, Comput. Math. Appl., 79 (2020), pp. 2021–2034, <https://doi.org/10.1016/j.camwa.2019.09.022>.
- [6] P. BASTIAN, M. BLATT, A. DEDNER, C. ENGWER, R. KLÖFKORN, R. KORNUBER, M. OHLBERGER, AND O. SANDER, *A generic grid interface for parallel and adaptive scientific computing. Part II: Implementation and tests in DUNE*, Computing, 82 (2008), pp. 121–138, <https://doi.org/10.1007/s00607-008-0004-9>.
- [7] L. BEIRÃO DA VEIGA, C. LOVADINA, AND G. VACCA, *Divergence free virtual elements for the Stokes problem on polygonal meshes*, ESAIM Math. Model. Numer. Anal., 51 (2015), pp. 509–535, <https://doi.org/10.1051/m2an/2016032>.
- [8] L. BEIRÃO DA VEIGA, F. BREZZI, A. CANGIANI, G. MANZINI, L. D. MARINI, AND A. RUSSO, *Basic Principles of Virtual Element Methods*, Math. Models Methods Appl. Sci., 23 (2013), pp. 199–214, <https://doi.org/10.1142/S0218202512500492>.
- [9] S. C. BRENNER AND L. R. SCOTT, *The mathematical theory of finite element methods*, no. 15, Springer, New York, 2008.
- [10] J. W. CAHN, *On spinodal decomposition*, Acta Metall., 9 (1961), pp. 795–801, [https://doi.org/10.1016/0001-6160\(61\)90182-1](https://doi.org/10.1016/0001-6160(61)90182-1).
- [11] J. W. CAHN AND J. E. HILLIARD, *Free energy of a nonuniform system. I. interfacial free energy*, J. Chem. Phys., 28 (1958), pp. 258–267, <https://doi.org/10.1063/1.1744102>.
- [12] A. CANGIANI, G. MANZINI, AND O. J. SUTTON, *Conforming and nonconforming virtual element methods for elliptic problems*, IMA J. Numer. Anal., 37 (2017), pp. 1317–1354, <https://doi.org/10.1093/imanum/drw036>.
- [13] F. CHAVE, D. A. DI PIETRO, F. MARCHE, AND F. PIGEONNEAU, *A hybrid high-order method for the cahn–hilliard problem in mixed form*, SIAM J. Numer. Anal., 54 (2016), pp. 1873–1898, <https://doi.org/10.1137/15M1041055>.
- [14] S. CHOO AND Y. LEE, *A discontinuous galerkin method for the cahn–hilliard equation*, J. Appl. Math. Comput., 18 (2005), pp. 113–126, <https://doi.org/10.1007/BF02936559>.
- [15] M. CROUZEIX AND V. THOMÉE, *The stability in L_p and W_p^1 of the L_2 projection onto finite element function spaces*, Math. Comp., 48 (1987), pp. 521–532, <https://doi.org/10.1090/S0025-5718-1987-0878688-2>.
- [16] A. DEDNER AND A. HODSON, *Robust nonconforming virtual element methods for general fourth-order problems with varying coefficients*, IMA J. Numer. Anal., (2021), <https://doi.org/10.1093/imanum/drab003>.

- [17] A. DEDNER, R. KLOEFKORN, AND M. NOLTE, *Python bindings for the DUNE-FEM module*, Zenodo, 10 (2020), <https://doi.org/10.5281/zenodo.3706994>.
- [18] A. DEDNER, R. KLÖFKORN, M. NOLTE, AND M. OHLBERGER, *A generic interface for parallel and adaptive discretization schemes: abstraction principles and the DUNE-FEM module*, Computing, 90 (2010), pp. 165–196, <https://doi.org/10.1007/s00607-010-0110-3>.
- [19] A. DEDNER AND M. NOLTE, *The DUNE-PYTHON module*, arXiv preprint arXiv:1807.05252, (2018).
- [20] D. A. DI PIETRO AND A. ERN, *A hybrid high-order locking-free method for linear elasticity on general meshes*, Comput. Meth. Appl. Mech. Engrg., 283 (2015), pp. 1–21, <https://doi.org/10.1016/j.cma.2014.09.009>.
- [21] I. C. DOLCETTA, S. F. VITA, AND R. MARCH, *Area-preserving curve-shortening flows: from phase separation to image processing*, Interfaces Free Bound., 4 (2002), pp. 325–343, <https://doi.org/10.4171/IFB/64>.
- [22] C. M. ELLIOTT, *The Cahn-Hilliard model for the kinetics of phase separation*, in Mathematical models for phase change problems, Springer, 1989, pp. 35–73, https://doi.org/10.1007/978-3-0348-9148-6_3.
- [23] C. M. ELLIOTT AND D. A. FRENCH, *Numerical studies of the Cahn-Hilliard equation for phase separation*, IMA J. Appl. Math., 38 (1987), pp. 97–128, <https://doi.org/10.1093/imamat/38.2.97>.
- [24] C. M. ELLIOTT AND D. A. FRENCH, *A nonconforming finite-element method for the two-dimensional Cahn-Hilliard equation*, SIAM J. Numer. Anal., 26 (1989), pp. 884–903, <https://doi.org/10.1137/0726049>.
- [25] C. M. ELLIOTT, D. A. FRENCH, AND F. MILNER, *A second order splitting method for the Cahn-Hilliard equation*, Numer. Math., 54 (1989), pp. 575–590, <https://doi.org/10.1007/BF01396363>.
- [26] C. M. ELLIOTT AND Z. SONGMU, *On the Cahn-Hilliard equation*, Arch. Ration. Mech. Anal., 96 (1986), pp. 339–357, <https://doi.org/10.1007/BF00251803>.
- [27] C. M. ELLIOTT AND A. STUART, *The global dynamics of discrete semilinear parabolic equations*, SIAM J. Numer. Anal., 30 (1993), pp. 1622–1663, <https://doi.org/10.1137/0730084>.
- [28] D. J. EYRE, *Unconditionally gradient stable time marching the Cahn-Hilliard equation*, MRS Online Proceedings Library (OPL), 529 (1998), <https://doi.org/10.1557/PROC-529-39>.
- [29] H. GÓMEZ, V. M. CALO, Y. BAZILEVS, AND T. J. HUGHES, *Isogeometric analysis of the Cahn-Hilliard phase-field model*, Comput. Methods Appl. Mech. Engrg., 197 (2008), pp. 4333–4352, <https://doi.org/10.1016/j.cma.2008.05.003>.
- [30] M. KÄSTNER, P. METSCH, AND R. DE BORST, *Isogeometric analysis of the Cahn-Hilliard equation—a convergence study*, J. Comput. Phys., 305 (2016), pp. 360–371, <https://doi.org/10.1016/j.jcp.2015.10.047>.
- [31] D. KAY, V. STYLES, AND E. SÜLI, *Discontinuous Galerkin finite element approximation of the Cahn-Hilliard equation with convection*, SIAM J. Numer. Anal., 47 (2009), pp. 2660–2685, <https://doi.org/10.1137/080726768>.
- [32] H. G. LEE, *Stability condition of the second-order SSP-IMEX-RK method for the Cahn-Hilliard equation*, Mathematics, 8 (2020), p. 11, <https://doi.org/10.3390/math8010011>.
- [33] X. LIU AND Z. CHEN, *A virtual element method for the Cahn-Hilliard problem in mixed form*, Appl. Math. Lett., 87 (2019), pp. 115–124, <https://doi.org/10.1016/j.aml.2018.07.031>.
- [34] X. LIU, Z. HE, AND Z. CHEN, *A fully discrete virtual element scheme for the Cahn-Hilliard equation in mixed form*, Comput. Phys. Commun., 246 (2020), p. 106870, <https://doi.org/10.1016/j.cpc.2019.106870>.
- [35] J. SHIN, H. G. LEE, AND J.-Y. LEE, *Unconditionally stable methods for gradient flow using Convex Splitting Runge-Kutta scheme*, J. Comput. Phys., 347 (2017), pp. 367–381, <https://doi.org/10.1016/j.jcp.2017.07.006>.
- [36] G. N. WELLS, E. KUHL, AND K. GARIKIPATI, *A discontinuous Galerkin method for the Cahn-Hilliard equation*, J. Comput. Phys., 218 (2006), pp. 860–877, <https://doi.org/10.1016/j.jcp.2006.03.010>.
- [37] S. ZHANG AND M. WANG, *A nonconforming finite element method for the Cahn-Hilliard equation*, J. Comput. Phys., 229 (2010), pp. 7361–7372, <https://doi.org/10.1016/j.jcp.2010.06.020>.
- [38] J. ZHAO, B. ZHANG, AND X. ZHU, *The nonconforming virtual element method for parabolic problems*, Appl. Numer. Math., 143 (2019), pp. 97–111, <https://doi.org/10.1016/j.apnum.2019.04.002>.